FUNDAMENTAL INVESTIGATION OF EXHAUST HOODS

FINAL REPORT

by

Nurtan A. Esmen
Principal Investigator
Dietrich A. Weyel
Co-Principal Investigators

T. A. Grauel III
A.G.Ilori
S. Jossell
A. Pirris

Department of Industrial Environmental Health Sciences
Graduate School of Public Health
University of Pittsburgh
130 Desoto Street
Pittsburgh PA 15261

Submitted to
National Institute of Occupational Safety and Health
Grant # RO1 OH02132 - 01 through RO1 OH02132 - 04

August 1990

TABLE OF CONTENTS

LIST OF FIGURES

LIST OF TABLES

SIGNIFICANT FINDINGS

While a number of theoretical and experimental findings lead to important results, the most significant results obtained in this research project was the observed effect of turbulence on the capture efficiency of hoods and the magnitude of the reduction of the capture efficiency with what might be considered to be a relatively mild turbulent cross draft. Experimental results showed that a turbulent cross draft (turbulence intensity of about 3 percent) in the order of 5 to 10 percent of the hood induced air speed in the mean velocity magnitude can reduce the overall capture efficiency of a hood by 15 percent.

The theoretical investigation of air flow in front of freely suspended flanged hoods with arbitrarily, but symmetrically shaped hood orifices was carried out by sink super imposition method developed as a part of this research project. The equations developed agree well with the experimental results. As a result of this study, a direct method of solution for any shape symmetric hood and approximate equations for regular shapes are now available.

The theoretical investigations were also extended to include hoods with adjacent planes of arbitrary orientation. Using a conformal mapping technique, complete equations which incorporate the presence of adjacent planes to airflow field calculations in front of hoods were developed.

Optimization techniques which consider the hood geometry were investigated. A simplified optimization technique was

developed and reported. The optimization technique developed may be used to select hood orifice shape and dimensions not only to achieve proper control but also improve the mechanical efficiency of the exhaust hood operation.

The theories developed were experimentally verified using up to date hot wire anemometry techniques. In addition, significant amount of hot wire anemometry data were collected for hood orifice shapes and flow conditions not yet analyzed or reported. Probably, one of the important achievements of this project is the experimental data accumulated over the extent of the project. The investigators are in the process of collating and tabulating this data. When this collating process is complete, the data will be made available to any interested party. The data collected includes turbulence measurements in the wake of blunt objects in front of a hood, flow profiles of multiple orifice hoods and turbulence intensities in the vicinity of the hood flanges generated by the suction of hoods.

ABSTRACT

The theoretical investigation of airflow in front of freely suspended flanged hoods with arbitrarily, but symmetrically shaped hood orifices suggests that an extension of the superimposition of two virtual sinks and potential flow assumption to describe the flow field can be used. Although the general solution may result in a rather complicated set of expressions, the specific solutions for circular, oblong and rhombic orifices give tractable solutions. The superimposition method also leads to a tractable solution for triangular orifices. The theoretical development reported here provides the basis for the generalized equations and presents the specific equations for circular, oblong, rhombic and triangular orifices.

The velocity profiles of flow fields generated by freely suspended exterior hoods with selected shape orifices were determined using hot wire anemometry. The experimental procedures used allowed the determination of the vector velocity field. The results of the experiments showed that the theoretical results reported here are accurate predictors of the velocity profiles within the restrictions of the potential flow assumptions.

Recent theoretical and experimental studies of the air flow field due to a freely suspended suction hood, published or reported here, have resulted in a number of important advances in the understanding of the flow field in front of a suction hood. In most industrial situations, an adjacent plane in addition to the flange of the hood is also present. In the original

consideration of adjacent planes, Fletcher and Johnson showed their significance in modifying the flow field and proposed a simple model to predict the centerline velocity of a hood with an adjacent plane. In this report the results of a theoretical and experimental study of oblong and circular orifice flanged hoods with one or two adjacent planes is presented.

The theoretical approach is based on contraction mapping of the flow field generated by an equivalent freely suspended hood. The experimental and theoretical results agree qualitatively over the entire flow field and agree quantitatively in the portions of the field where the potential flow assumption is valid.

The two most important concerns in the design of exterior hoods are to achieve maximum hood capture efficiency with minimum flow rate. Often, these two concerns operate in opposite directions for a fixed hood geometry and capture surface geometry. Thus, for a given capture surface specification, the flow rate to achieve the specifications would have to consider the geometry of the hood surface in order to seek an optimum solution. The results presented in this report considers the effect of changes in hood geometry on the velocity field for a given capture surface specification.

The use of local and general exhaust systems is common practice in the control of many different types of environmental contaminants from heat to toxic dusts. The new approaches to hood design allow the characterization of the entire flow field in front of the hood. The last phase of the investigation looked at

the effects of a superimposed turbulent cross draft on the capture efficiency of a flanged circular orifice exhaust hood. It was found that turbulence of the type typically seen in the flow of air around blunt objects, such as the body or extremities of a worker in the flow field, causes a significant reduction in capture efficiency. A theoretical explanation of the reduction of capture efficiency brings into question the validity of the current criteria used in hood design.

In addition to the main research findings reported, several, albeit minor, findings are also reported.

MAIN RESULTS OF RESEARCH

A. Theoretical and Experimental Investigation of Unobstructed Exhaust Hoods:

In the design or selection of exterior hoods, the velocity profile in front of the hood is of prime importance; because it determines the capture efficiency of that hood. In several recent investigations (ESMEN et al.1986; FLYNN and ELLENBECKER 1985) theoretical and experimental analyses of velocity profiles in front of flanged hoods with oblong orifices with and without adjacent planes, and flanged hoods with circular orifices without adjacent planes were reported. In addition, a recent article by BRACONIER (1986) provided an excellent review of experimental and theoretical studies of hoods. The results reported in these papers suggested that a simple linear approach of estimating the centerline velocity is not a sufficient determinant for efficient hood design. This suggestion was further confirmed by the results reported by Flynn and Ellenbecker (1986) on a study pertaining to the capture efficiency of flanged, circular orifice local exhaust hoods. In order to evaluate the economic and capture efficiency of a hood one must first define the fluid mechanical efficiency. This parameter may be defined as the air flow required to satisfy a specified set of air velocities at specific points in front of the hood. With such a definition, it may be shown that the linear centerline velocity based hood selection often will lead to poor fluid mechanical efficiency as well as poor capture efficiency (ESMEN and WEYEL 1986). In this work, it was also shown that

flanged hoods with multiple oblong openings can improve both, the theoretical capture efficiency and the fluid mechanical efficiency of a hood.

The last observation above suggests possibilities in the design of exterior hoods such that an optimum set of openings may be utilized to improve capture efficiency and fluid mechanical efficiency as well as address the problems poor capture efficiency caused by cross drafts. Although the results hitherto available may be used to investigate these possibilities, it is important to point out that the shape of the openings selected may also influence the possible optimization processes. Thus, availability of solutions for two shapes only may not be sufficient for the full consideration of optimization. In order to consider the full implications of different shapes, a general theoretical approach to the flow field in front of a flanged hood with an arbitrarily shaped orifice was developed.

In the theoretical development, flanged hoods with an arbitrary but symmetric orifice are considered. It is also assumed that the flange of the hood is sufficiently large to be considered infinite in extent. It is further assumed that the hood is freely suspended; consequently, there is no adjacent plane in the vicinity of the hood. As will be shown, the specific expressions obtained for symmetric shapes may be extended to equilateral triangle shaped orifices and provide a basis for design calculations using oblong, circular, triangular and rhombic hood openings. In addition to design considerations in

quiescent rooms, the theoretical development provides expressions which fully specify the flow field in front of the hood; thus,the results may be used in the investigation of the interaction between hood suction and cross draughts, flow fields due to multiple openings, and hood capture efficiency.

Theoretical Considerations

The basis of the theoretical development given below is the applicability of the potential flow theory to flanged orifices. If the velocities generated by the hood orifice is assumed to be due to the irrotational flow of an inviscid and incompressible fluid, then the velocity potential for the flow field satisfies Laplace's equation. Thus the governing equation of the flow is a linear partial differential equation and consequently various solutions of Laplace's equation may be used in combination to express the velocities generated by the fluid flow. Such a combination process is called super imposition. The superimposition process enables one to build complicated flow patterns from simple solutions.

In order to apply these concepts to exhaust hood flow, consider an orifice with a constant magnitude face velocity, V_0 located at the origin of a Cartesian coordinate system and consider the orifice to be symmetric with respect to both z and y axes but otherwise arbitrary in shape. Consider an arbitrary point P (x,y,z) the induced velocity vector V(x,y,z). The velocity vector may be resolved into two vectors one on a plane

Pz which contains the point P and the z axis and another on a plane which contains the point P and the y axis. Consequently, any point in front of the orifice may be identified by means of two characteristic planes and a point on each plane and the velocity vector may be found through the analyses of two dimensional potential flow on two planes. The general approach to the analyses of the problem on either plane is the same.

Consider the two dimensional potential flow for a point P located in front of the orifice as shown in figure 1. It may be observed that the velocity potential at point P is equivalent to the sum of the contributions of sinks with sink strength m(l) located between -a and a. By defining the sign function sg(Y) to be the sign of Y, the components of the velocity contributed by each sink may be expressed as:

$$V_X(P,r) = -\frac{m(l)\,(X + f(Y))}{2\pi\, r^2(l)} \tag{1}$$

$$V_Y(P,r) = -\frac{m(l)\,(||Y|| - l)}{2\pi\, r^2(l)}\, sg(Y) \tag{2}$$

with

$$r^2 = (||Y|| - 1)^2 + X^2 + a^2 \tag{3}$$

and

$$f(Y) = \begin{cases} 1 & ||Y|| < a \\ 0 & ||Y|| > a \end{cases} \tag{4}$$

Due to the symmetry V_Y (Y<0) is equal to V_Y (Y>0) in magnitude but opposite in sign, in the development only the right half plane can be considered without loosing generality. In order to simplify the development, the space variables may be divided by

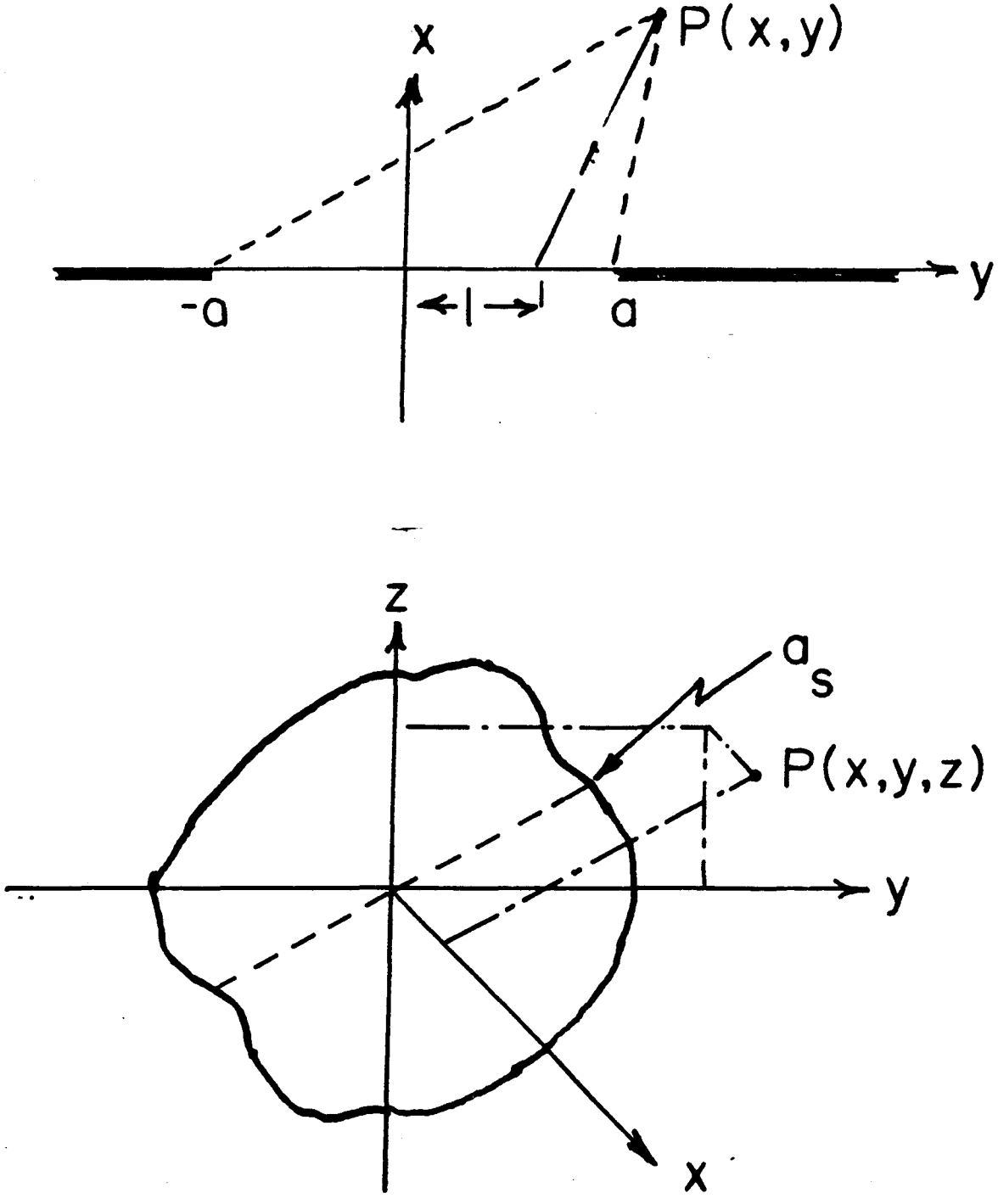

Figure 1. Schematic diagram of a hood opening and an arbitrary point used in the theoretical development

a to obtain dimensionless distances. In the equations below the distances shown with a superscript o are dimensionless variables. Summing over all possible sinks on the line, V(P) may be expressed as:

$$V(P) = \int_{-1}^{1} \frac{\partial V}{\partial l^{o}} \, dl^{o} \qquad (5)$$

By the use of the mean value theorem twice, with $-1 < \sigma, \gamma < 1$ the components of the velocity at P may be written as:

$$V_X(P) = \frac{-m(\sigma)}{2\pi a} \cdot \frac{\arctan \dfrac{||Y^{o}|| + 1}{X^{o} + 1} - \arctan \dfrac{||Y^{o}|| - 1}{X^{o} + 1}}{X^{o} + 1} + \frac{X^{o}}{2\, r^{2}(\gamma)} \int_{-1}^{1} \frac{\partial m}{\partial l^{o}} \, dl^{o} \qquad (6)$$

$$f(Y^{o}) = \begin{cases} 1 & Y^{o} < 1 \\ 0 & Y^{o} > 1 \end{cases} \qquad (7)$$

$$V_Y(P) = \frac{-m(\sigma)}{2\pi a} \cdot \frac{1}{2} \ln \left[\frac{r^{2}(-1)}{r^{2}(1)} \right] + \frac{Y - \gamma}{2r^{2}(\gamma)} \int_{-1}^{1} \frac{\partial m}{\partial l^{o}} \, dl^{o} \qquad (8)$$

With $m(\sigma)$= representative sink strength; boundary conditions suggest that if X = 0 and Y = 0, then V_X = constant and V_Y = 0. Similarly, if X = 0 and Y = a , then V_Y = constant. These two conditions may be used to calculate the values of the integral, $m(\sigma)$ and γ of equations above. After a few algebraic steps, with the orifice speed U_0 , these equations may be rewritten as:

$$\frac{V_X}{U_0} = -\frac{\arctan \dfrac{||Y^{o}|| + 1}{[X^{o} + f(Y^{o})]^{2}} - \arctan \dfrac{||Y^{o}|| - 1}{[X^{o} + f(Y^{o})]^{2}}}{2 \arctan(1) \, [X^{o} + f(Y^{o})]} + \frac{X^{o}}{r^{2}(\gamma)} \int_{-1}^{1} \frac{\partial m}{\partial l^{o}} \, dl^{o} \qquad (9)$$

$$V_X = -\frac{U_0\,(X^o + f(Y^o))}{8}\left[\frac{1}{r^2(1)} - \frac{1}{r^2(-1)} + \frac{8}{5\,r^2(0)}\right] \qquad (10)$$

$$V_Y = -2\,U_0\left[\ln\left[\frac{r^2(-1)}{r^2(1)}\right] + \frac{2\,Y^o}{r^2(0)}\,(1 - \ln(5)/2)\right] sg(y) \qquad (11)$$

with,

$$f(Y^o) = \begin{cases} 1 & Y^o < 1 \\ 0 & Y^o > 1 \end{cases} \qquad (12)$$

$$X^o = \left[\frac{x^2 + z^2}{a^2}\right]^{1/2} \qquad (13)$$

and

$$r^2(b) = \left[\,\| Y^o \| - b\,\right]^2 + \left[X + f(Y)\right]^2 \qquad (14)$$

For the general three dimensional case, the treatment of the flow involves the consideration of two characteristic planes. Consequently, equations 10 through 14 may be directly extended to the three dimensional case by defining the dimension of the orifice in each plane and by modifying the f(Y) to f(y,z). With these modifications, the components of the velocity vector at point P may be given as:

$$V_x = V_{X_y}\,\frac{(x + a_s\,f(y,z))/2}{\left[\,(x + a_s f(y,z))^2 + z^2\,\right]^{1/2}} + V_{X_z}\,\frac{(x + a_s\,f(y,z))/2}{\left[\,(x + a_s f(y,z))^2 + y^2\,\right]^{1/2}} \qquad (15)$$

$$V_y = V_{X_z}\,\frac{y/2}{\left[\,(x + a_s\,f(y,z))^2 + y^2\,\right]^{1/2}} + V_Y/2 \qquad (16)$$

$$V_z = V_{X_y}\,\frac{z/2}{\left[\,(x + a_s\,f(y,z))^2 + z^2\,\right]^{1/2}} + V_Z/2 \qquad (17)$$

where,

$$f(y,z) = \begin{cases} 1 & (0,y,z) \in \text{orifice surface} \\ 0 & \text{Elsewhere} \end{cases} \qquad (18)$$

The development of the equations which describe the velocity in front of a symmetric hood by the direct procedure shown above leads to rather cumbersome equations. However, this development suggests that the magnitude of the velocity may be related to appropriately chosen representative sinks. Thus by the use of the mass balance for a constant density gas, alternate approximate expressions may be developed. Let Ar(x,y,z) be the surface generated by all points such that the magnitude of the corresponding vector velocity is a constant and the velocity vector is normal to the surface. The mass balance suggests that the mass flow across this surface must equal to the mass flow across the surface of the orifice. Therefore, for a constant density gas:

$$Ar_o \, \| \, V_o \| = Ar(x,y,z) \, \| \, V(x,y,z) \, \| \qquad (19)$$

where,

V_o = Hood face velocity.

$V(x,y,z)$ = Velocity at point x,y,z.

Ar_o = Area of the orifice surface S_o .

$Ar(x,y,z)$ = Area of the surface defined by $\| V(x,y,z) \|$ is a constant (iso-kinetic surface).

Equation 19 suggest that the magnitude of the velocity may be determined by a function which scales the orifice area to the area of the iso-kinetic surface. If every point on Ar(x,y,z) is

mapped unto the surface of the orifice, the mapping function may be used as the parameter of a scaling functional to determine the magnitude of the velocity at the corresponding point. With this procedure, the relationship between the velocity at any point and the hood velocity may be given as:

$$V(x,y,z) = \{ \| V_0 \| / f(R) \} D \qquad (20)$$

where,

$\| V_0 \|$ = Magnitude of the face velocity

D = Directional vector as determined by the sum of vectors leading to the characteristic sinks.

R = Orifice geometry dependent position function

f(R) = Orifice geometry dependent scaling functional

It may be noted that the direct equations are related to the minimum and maximum distance between the point and the hood surface and the maximum distance is related to minimum. Consequently, the maximum distance is a function of the minimum distance and the distance to the geometric center of the hood orifice. Therefore, appropriately scaled sinks located at these points may be used to define the velocity vector at the point of interest. The characteristic attributes of the vector velocity V(x,y,z) are determined by these characteristic sinks and scaled by the relationship shown in equation 19. Therefore, the iso-kinetic surface may be taken as the parametric surface generated by all points with the associated parameter $\| V(x,y,z) \|$ equal to a scalar constant and since the constant which represents representative sink strength is the same for both sides of the

equation, then it can be factored out of the norms of the vectors on both sides. Consequently, equation 20 may be used to determine the value of the magnitude of the velocity at any given point. The area of the iso-kinetic surface can be readily calculated based on the geometry of the orifice. If the norm of the vector defined by equations 15 - 18 is a constant, say C then, x may be expressed as a function of y,z and C. Thus,

$$Ar(x,y,z,\| V(x,y,z) \|) = \iint_S \left[1 + \left[\frac{x}{y}\right]^2 + \left[\frac{-x}{z}\right]^2\right]^{1/2} dz\, dy \quad (21)$$

For any general hood surface, the evaluation of this integral might present problems. The simplest approach to the evaluation of the integral over a chosen shape is to divide the integration surface into several simply connected regions. One of these regions is the surface of the orifice and the others may be selected conveniently to simplify the algebraic manipulations in the development of the final equation. Also, in order to carry out the integration, the surface must be shown to possess derivatives of at least two orders. It may be noted that the parametric surface is generated by solutions of Laplace's equations associated with sinks located on the orifice surface and the plane orthogonal to the hood which shares the straight line connecting the sinks. The velocity function is determined by the solutions of the Laplace's equation in two dimensions and it may be shown to be holomorphic in this domain (Menchoff(1936); Bers and Gelbart(1944)). The same argument is true for any two arbitrary points on the iso-kinetic surface and clearly, the

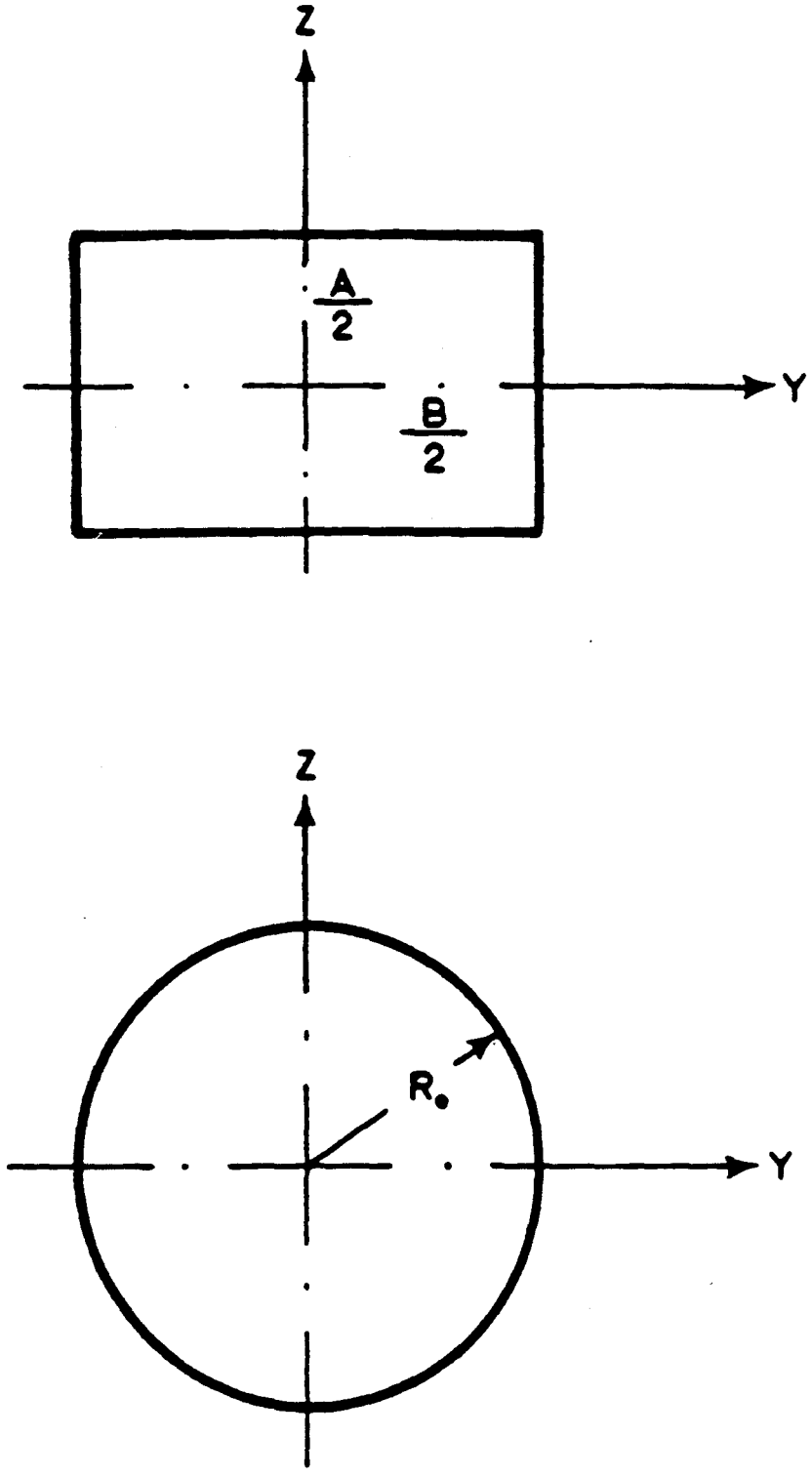

Figure 2. Orientation and Parameters of Circle and Oblong Orifices.

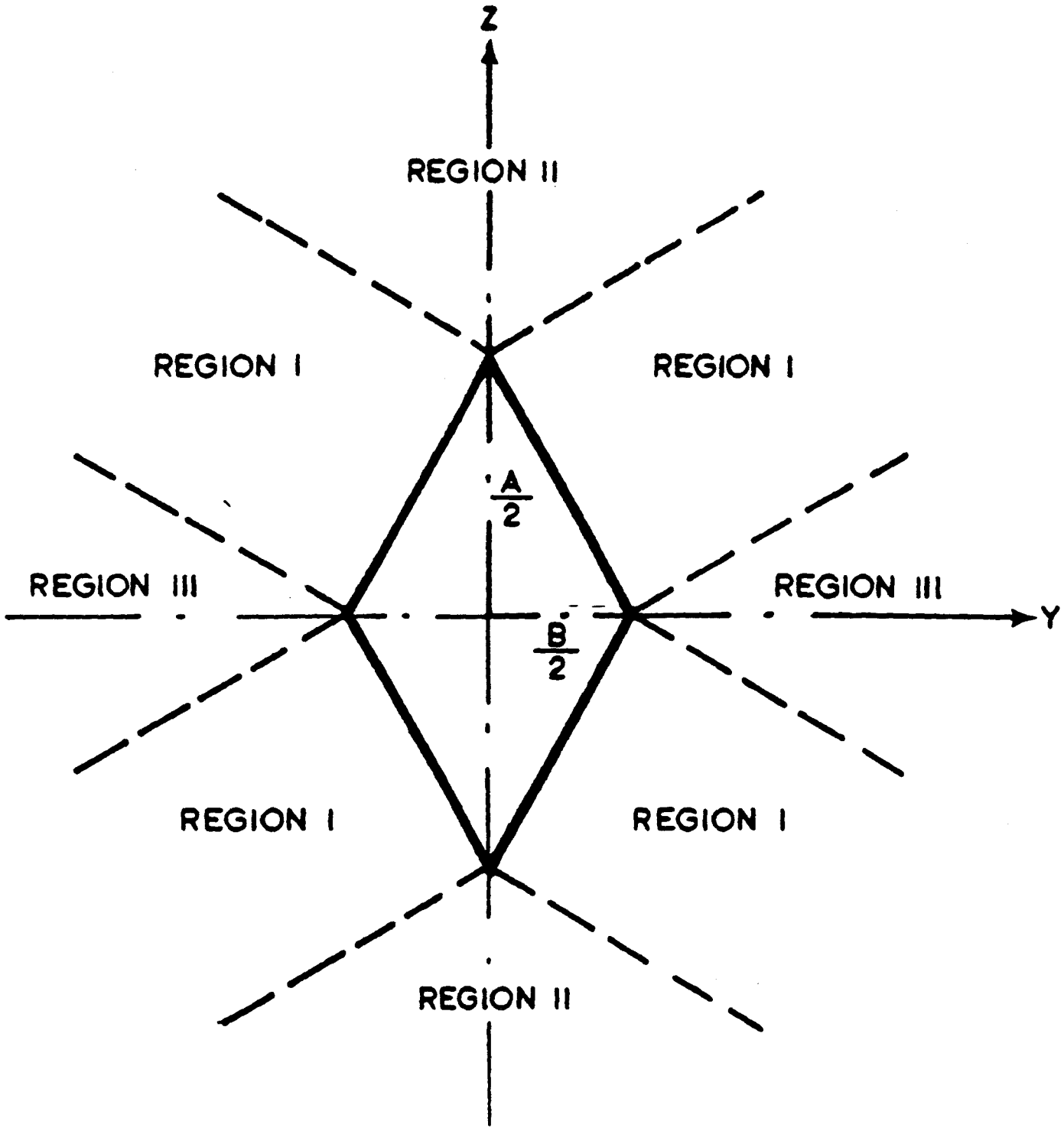

Figure 3. Orientation and Parameters of Rhombus Orifice.

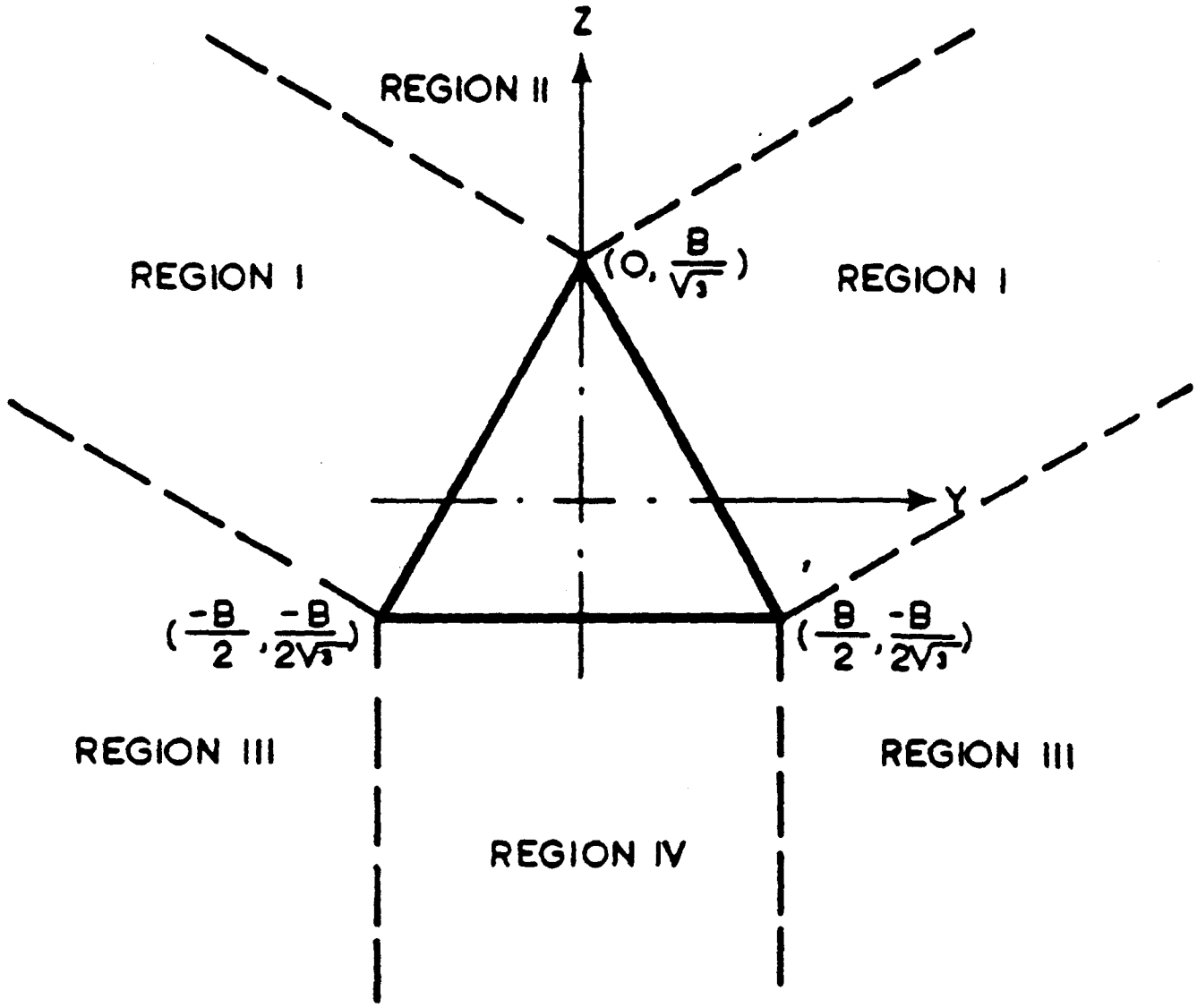

Figure 4. Orientation and Parameters of Triangle Orifice.

intersection of these two domains is not empty. Therefore, it may be shown that each function is an analytic continuation of the other and the derivatives of at least two orders exist on the surface. Consequently, the only difficulty in the evaluation of the integral comes from the choice of the hood orifice shape. However, for symmetric orifice surfaces this problem is considerably reduced by direct geometric constructs in the determination of the integral.

The profile of the two dimensional flow in the domain of the characteristic plane defined above is the case of a fluid flowing into an aperture. Thus the potential lines, (the orthogonal lines to stream lines) are confocal ellipses (Lamb (1945)). If this plane is rotated about an axis passing through the center of the orifice, the surface generated by a constant potential line is the surface generated by the rotation of ellipses resulting from potential flow solutions of a uniformly varying aperture. The area of the surface defined by these potential lines which correspond to a constant velocity magnitude may be approximated readily, because this surface as a functional of a position function leads to rather simple geometric constructs.

The equations developed for flanged hoods with oblong orifices was reported previously (ESMEN et al. 1986) and it is included here for the sake of completeness. The equation shown in this paper is identical to the previously reported equation, except that it does not contain the provisions for an adjacent plane as was given before. For the equations presented below, the

unit vectors e_x, e_y, e_z refer to x,y,z directions respectively.

Consider a hood with an oblong orifice and its attendant coordinate system origin (0,0,0) located at the center of the orifice. Let the orifice be defined by the area $-A/2 < z < A/2$; $-B/2 < y < B/2$ as shown in Figure 2. The scaling functional for such a geometry for all positive values of x may be shown to be:

$$f(R) = \frac{\pi R}{2AB}\left[A + B + 4\pi R \right] + \left[1 + \frac{4(||yx|| + ||zx||)}{A^2 + B^2} \right]^{1/2} \qquad (22)$$

with the position function given as:

$$R^2 = x^2 + k_y \left(||y|| - B/2\right)^2 + k_z \left(||z|| - A/2\right)^2 \qquad (23)$$

With,

$$k_y = \begin{cases} 0 & ||y|| < B/2 \\ 1 & \text{Elsewhere} \end{cases} \qquad (24)$$

$$k_z = \begin{cases} 0 & ||z|| < A/2 \\ 1 & \text{Elsewhere} \end{cases} \qquad (25)$$

and finally, from the sum of the vectors pointing to the virtual sinks, the directional vector may be expressed with the aid of an auxiliary position vector, P :

$$P = 4(x+k_x)\, e_x + |2y(k_y+1) - sg(y)B\, k_y|\, e_y + |2z(k_z+1) - sg(z)A\, k_z|\, e_z \qquad (26)$$

where,

$$k_x = \begin{cases} 1 & y,z \in \text{orifice co-ordinates} \\ 0 & \text{Elsewhere} \end{cases} \qquad (27)$$

and with e_x, e_y, e_z unit vectors in x,y,z directions respectively. The direction of P gives the directional vector D:

$$D = -P / (P.P)^{1/2} \qquad (28)$$

For a flanged hood with a circular orifice of radius R_0 and the coordinate system origin located at the orifice center as shown in Figure 2, the scaling functional may be expressed as:

$$f(R) = \frac{\pi R}{2 R_0} \left[1 + \frac{R}{R_0} \right] + \left[1 + \frac{4 x \sqrt{y^2 + z^2}}{(\pi^2 - 2\pi) R_0^2} \right]^{1/2} \qquad (29)$$

The position function may be expressed as:

$$R = x^2 + k_r \left[(L - R_0)^2 \right] \qquad (30)$$

with,

$$k_r = \begin{cases} 0 & y^2 + z^2 < R_0^2 \\ 1 & \text{Elsewhere} \end{cases} \qquad (31)$$

and

$$L = \sqrt{y^2 + z^2} \qquad (32)$$

As above, the directional vector is defined with the aid of vector P and the directional vector D (eq. 28) as:

$$P = 2(1+k_x) x\, e_x + \left[1 + k_r \left(1 - \frac{R_0}{L} \right) \right] (y\, e_y + z\, e_z) \qquad (33)$$

The analysis of a flanged hood with a rhombus shaped orifice can be carried out by defining three distinct regions as shown in Figure 3. It must be noted that these regions are not unique and were chosen somewhat arbitrarily, by trial and error, for the ease of performing the integration required. Their choice will effect only the position function and any other set of regions chosen would give an equivalent position function without

changing the form of the scaling functional. The three regions chosen are defined by the following inequalities:

Region I : $-B^2 < 2A\|z\| - 2B\|y\| < A^2$

and

$$2A\|y\| + 2B\|z\| > AB$$

Region II : $2A\|z\| - 2B\|y\| > A^2$

Region III : $2A\|z\| - 2B\|y\| < -B^2$

Using these regions, the scaling functional for a rhombus shaped orifice may be written as:

$$f(R) = \frac{R}{AB}\left[\sqrt{A^2+B^2}+4R\right] + \left[1 + \frac{4(\|xy\| + \|xz\|)}{A^2 + B^2 - AB}\right]^{1/2} \quad (34)$$

With the position function:

$$R^2 = x^2 + k_1\left(\|y\| - \frac{B}{2} + \frac{B}{A}\|z\|\right)^2 \frac{A^2}{A^2+B^2} + k_2\left[\left(\|z\| - \frac{A}{2}\right)^2 + y^2\right] + k_3\left[\left(\|y\| - \frac{B}{2}\right)^2 + z^2\right] \quad (35)$$

with

$$k_1 = \begin{cases} 1 & y,z \subset \text{Region I} \\ 0 & \text{Elsewhere} \end{cases} \quad (36)$$

$$K_2 = \begin{cases} 1 & y,z \subset \text{Region II} \\ 0 & \text{Elsewhere} \end{cases} \quad (37)$$

$$k_3 = \begin{cases} 1 & y,z \subset \text{Region III} \\ 0 & \text{Elsewhere} \end{cases} \quad (38)$$

As above:

$$P= 2(x+k_x)\, e_x + y(1 + k_2) + k_1\, sg(y)[||y||+(B/A)||z|| - B/2] \frac{A^2}{A^2 + B^2}$$

$$+ k_3\, sg(y)(||y|| - B/2)\, e_y + z(1 + k_3) + k_2\, sg(z)(||z|| - A/2)$$

$$+ k_1\, sg(z)[||y||+(B/A)||z||-B/2] \frac{AB}{A^2 + B^2}\, e_z \qquad (39)$$

The flow field equations for a flanged hood with an equilateral triangular orifice are more complicated in the definition of the mapping regions, thus the position function R and the directional vector D can only be expressed by complicated equations. However, the equation for the scaling functional is sufficiently simple and as expected follows the general form of the equation found for the other geometries. In the construction of integration regions for an equilateral triangle shaped opening it was necessary to define four regions (Figure 4). These regions are described by:

Region I : $3||y|| + z\sqrt{3} > B$ and $-B < z\sqrt{3} - ||y|| < B$

Region II : $z\sqrt{3} - ||y|| > B$

Region III : $2||y|| > B$ and $z\sqrt{3} - ||y|| < -B$

Region IV : $2||y|| < B$ and $2z\sqrt{3} < -B$

The equation for the scaling functional resulting from these regions may be written as:

$$f(R)= \frac{2\pi R}{B\sqrt{3}} \left[3 + \frac{2R}{B} \right] + \left[1 + \frac{16\ (||xy||+||xz||)}{(9 - 2\sqrt{3})\ B^2} \right]^{1/2} \qquad (40)$$

with the position function:

$$R^2 = x^2 + k_1 \left[3\,||y|| + z\sqrt{3} - B \right]^2/12 + k_2 \left[\left(z - \frac{B}{\sqrt{3}} \right)^2 + y^2 \right]$$

$$+k_3 \left[\left(z + \frac{B}{2\sqrt{3}} \right)^2 + \left(||y|| - \frac{B}{2} \right)^2 \right] + k_4 \left[||z|| - \frac{B}{2\sqrt{3}} \right]^2 \qquad (41)$$

with,

$$k_1 = \begin{cases} 1 & y,z \subset \text{Region I} \\ 0 & \text{Elsewhere} \end{cases} \qquad (42)$$

$$k_2 = \begin{cases} 1 & y,z \subset \text{Region II} \\ 0 & \text{Elsewhere} \end{cases} \qquad (43)$$

$$k_3 = \begin{cases} 1 & y,z \subset \text{Region III} \\ 0 & \text{Elsewhere} \end{cases} \qquad (44)$$

$$k_4 = \begin{cases} 1 & y,z \subset \text{Region IV} \\ 0 & \text{Elsewhere} \end{cases} \qquad (45)$$

As above:

$$P = 2(x+k_x)\, e_x + y(1+k_2) + k_1\, sg(y)\, ||\left[3\,||y|| + z\sqrt{3} - B\right]/4\,||$$

$$+ k_3\, sg(y)\left(||y|| - \frac{B}{2}\right) e_y + z + k_2 \left(z - \frac{B}{\sqrt{3}}\right) + k_3 \left(z + \frac{B}{2\sqrt{3}}\right)$$

$$-k_1\, ||\left[3\,||y|| + z\sqrt{3} - B\right]\sqrt{3}/12\,|| + k_4 \left(z + \frac{B}{2\sqrt{3}}\right) e_z \qquad (46)$$

The evaluation of the equations presented above do not present special problems. If the velocities at a few points in front of a hood are to be found, the calculations can be carried out readily with a hand calculator. Although the determination of the entire field would require the use of a micro-computer, the computer program required to carry out the calculations is simply a point by point independent evaluation of the equations and require no special programming considerations.

The experimental evaluation of the equations developed for flanged hoods with an oblong orifice was reported in a previous paper (ESMEN et al.,1986). In addition, there are empirical semi-empirical and theoretical values for the flow field generated by a circular orifice hood. Dallavalle (1930) expressed the centerline velocity of a free circular hood by an empirical equation which has been well confirmed (Braconier;1986). In order to compare the theoretically obtained equations reported here with the ones reported by Flynn and Ellenbecker (1985,1987) and the empirical correlation of Dallavalle, the evaluation of the equations for the total velocity magnitude in the flow field or the magnitude of the centerline velocity was carried out for a circular orifice with a radius of 4 units . The results of this comparison is shown in Table 1. As it can be seen from this table, the agreement between these formulations are good.

Experimental Verification of The Theory

The data found in the literature were insufficient for the detailed confirmation of the theoretical equations; therefore, an experimental study to validate the theoretically determined equations was undertaken. The experimental hood system used in the study is a part of an experimental ventilation system which is capable of generating well controlled volumetric airflow rates up to 1 m^3/sec. The experimental, freely suspended hood consists of a cubic transition piece which acts as a plenum with the hood face attached. The plenum is suspended sufficiently far from any

TABLE 1

COMPARISON OF THEORETICAL MODELS FOR A CIRCULAR ORIFICE HOOD

Position		Ratio of Magnitudes Velocity Face Velocity / Point Velocity					
Axial	Rad	This work		Flynn & Ellenbecker			Dallavalle
		I.	II.	Model2	Model3	Semi-emp	
0.125	0	1.050	1.051	1.156	1.005	1.219	1.012
	2	1.103	1.059	1.157	1.007	1.216	*
	4	1.154	1.068	1.227	1.110	0.588	*
	6	2.137	2.207	3.776	3.762	4.417	*
	8	3.557	4.178	7.301	7.298	8.559	*
0.25	0	1.101	1.104	1.163	1.017	1.226	1.034
	2	1.205	1.122	1.166	1.023	1.217	*
	4	1.300	1.139	1.301	1.203	0.738	*
	6	2.278	2.241	3.787	3.773	4.428	*
	8	3.732	4.218	7.309	7.306	8.567	*
0.5	0	1.209	1.221	1.190	1.059	1.254	1.099
	2	1.408	1.225	1.202	1.076	1.230	*
	4	1.578	1.288	1.453	1.379	1.074	*
	6	2.539	2.326	3.829	3.816	4.474	*
	8	4.040	4.309	7.340	7.338	8.598	*
1	0	1.442	1.491	1.296	1.197	1.366	1.283
	2	1.811	1.558	1.338	1.248	1.351	*
	4	2.101	1.622	1.778	1.729	1.724	*
	6	3.028	2.560	3.993	3.980	4.633	*
	8	4.576	4.536	7.465	7.462	8.723	*
2	0	1.982	2.178	1.707	1.654	1.799	1.813
	2	2.641	2.309	1.833	1.786	1.917	*
	4	3.104	2.426	2.526	2.499	2.733	*
	6	4.005	3.251	4.585	4.575	5.237	*
	8	5.568	5.174	7.951	7.949	9.217	*
4	0	3.356	4.142	3.264	3.246	3.441	3.330
	2	4.478	4.390	3.534	3.519	3.749	*
	4	5.178	4.596	4.518	4.508	4.893	*
	6	6.131	5.355	6.556	6.552	7.299	*
	8	7.677	7.160	9.777	9.778	11.104	*
8	0	7.283	10.425	9.304	9.304	9.807	7.683
	2	9.113	10.879	9.708	9.709	10.272	*
	4	10.158	11.222	10.963	10.965	11.722	*
	6	11.269	11.999	13.159	13.163	14.275	*
	8	12.827	13.703	16.372	16.379	18.031	*

adjacent plane so that the flow field may be considered to be free from obstructions. The ventilation laboratory was rendered to quiescent conditions by blocking all of the nearby building ventilation inlets and outlets during the experiments. The air flow generated by the experimental ventilation system was recirculated into the room through a large outlet approximately 8 meters away from the experimental location. So far as it could be measured, the cross currents and room air currents were negligible compared to the velocities generated by the hood suction. Only when the velocity measurements were under 30 cm/sec, the effect of the room air currents was apparent. Three orifices (a rhombus, a circle and an equilateral triangle) with shapes which corresponded to those used in the theoretical development were used. An oblong orifice was not selected for the experimental investigation, because it is a special case of a parallelogram and thus related to the rhombus. In addition, experimental data for an oblong orifice was previously reported (Esmen et al.,1986). The rhombus had its major axis (12cm) vertically and its minor axis (8 cm) horizontally. The circle radius was 4.6 cm and the equilateral triangle was 8.9 cm on each edge. These orifices were manufactured in four rigid plastic face plates which could be installed on the hood plenum and readily exchanged as the experimental situation demanded. Each orifice was located approximately at the center of the face plate so that the possibility of the influence of the location of the orifice with respect to the sides of the plenum on the orifice

face velocity distribution was minimized. Subsequent investigation showed that this precaution was not necessary; the size of the inlet plenum as compared to the sizes of orifices used assured the uniform distribution of the velocities at the face plane of the orifice.

The velocity measurements of the flow field generated by the hood suction were made with an X probe hot film anemometer. This probe had two sensors in a configuration such that the sensors were at 45 and 315 degrees to two components of the flow and orthogonal to the third component. The anemometer probe was mounted on a sliding support with a scale accurate to 0.5 mm. This probe support system was approximately 45 cm from the nearest edge of the orifice, so that any disruption of the flow field was eliminated. The sliding support system assured accurate measurement of the coordinate points and replication of measurements after moving the probe showed excellent reproducability.

Hot wire or hot film anemometry is the most appropriate instrumentation for the analysis of the structure of a flow field. The sensor of the instrument is very sensitive over a large span of velocities and in addition the sensor is highly directional; thus, by the simultaneous use of multiple sensors, the vector velocity components can be determined directly and accurately. In this study a multi channel anemometer system (Thermo Systems Inc. IFA-100) was used.

The use of the thermal anemometer presupposes the careful

calibration of the instrument in an essentially uni-directional flow field. The calibration of the anemometer was carried out using a calibration tube designed for this purpose. The calibration tube consisted of a metering, sharp-edged orifice plate, leading into a flow straightening and then to a converging section. The end of the converging section was shielded approximately 1 cm away from the centerline to prevent cross currents. A 1 cm radial distance from the sensors was sufficient to prevent radiant heat loss from the heated probe. The air supply to the calibrator was filtered compressed air. The air temperature was determined during the calibration so that temperature corrections during the experiments could be made. The initial calibration of the calibration tube was carried out by calibrating the metering orifice against a spirometer and the uni-directionality of the flow was ascertained by placing a single strand hot wire anemometer at the center of the flow in a way that the sensing element was parallel to the flow tube. Under this circumstance, no velocity was indicated. The sensor was then rotated in small steps and it was observed that a maximum response (both horizontally and vertically) was reached when the sensor was 90 +/- 1 deg. with respect to the flow axis. The calculated velocity of the calibrator was further verified by comparing the calculated calibrator center line velocity values to the values obtained by a miniature pitot static tube placed along the calibrator centerline. This comparison showed that the calculated values were within the accuracy of pitot static

measurements i.e. precision obtainable in the measurement of the pressure differential given by the pitot static tube. The distribution of the velocity was essentially constant for radial distances up to 4 mm, thus the calibrating flow was assumed to be uni-directional and uniform. The anemometer probes used were calibrated to the full extent initially or when a probe was replaced due to breakage. In addition, a few calibration checks on each sensor were performed occasionally to ensure that the calibration was constant.

Experimental Design

In these experiments, the aim of the measurements was to verify the theoretically developed equations; thus the selection of the points of measurement were similar for all experiments guided by the convenience of the actual measurement rather than a preset scheme. However, sufficiently diverse areas in front of the orifice were investigated to ensure that the entire velocity field was represented. Before the selection of the experimental points, preliminary measurements were taken on a fixed plane, orthogonal to the x-axis on points systematically covering the plane at 2 cm intervals in both y and z directions. Once the symmetry of the measurements was established, the experimental points were selected at 35 or more locations on each plane only in the upper left quadrant of the coordinate system for circular and rhombic orifices, and in the entire left quadrants for the triangular orifice. The face velocity of the orifice was

determined by making initial measurements at every 0.5 cm interval grid point and subsequently verifying this value at one or two points on the x=0 plane. The value of the face velocity was determined at the beginning and the end of each day of experimentation. Although we did not observe changes in the face velocity more than 1 percent throughout the day, in about one half of the experiments, face velocities were determined several times during the course of the experiment. This measurement scheme was applied to all three orifice shapes studied.

The determination of the components of the velocity may be readily carried out by recording the velocity indicated by the two sensors of the anemometer and rotating the probe on its axis precisely 90 degrees without changing the point of measurement and repeating the measurement process. This method indicates four effective velocity measurements for the point under consideration. These measurements result in four, non-linear equations with six unknowns, namely the three velocity components of the point, approach angle (a) and the two probe parameters. If the alignment of the probe is such that the crossed sensor plane is parallel to one of the measurement planes as precisely as possible, then one of the probe parameters (h) may be assumed to be a constant near unity with a value as determined in the calibration and the other to be negligible (Jorgensen,1971), leaving four unknowns and four equations (Comte-Bellot,1976):

$$V_1^2 = (V_y \text{ Sin } a + V_z \text{ Cos } a)^2 + (h_1 V_x)^2 \qquad (42)$$

$$V_2^2 = (V_y \text{ Cos } a - V_z \text{ Sin } a)^2 + (h_2 V_x)^2 \quad (43)$$

$$V_3^2 = (V_y \text{ Sin } a + V_x \text{ Cos } a)^2 + (h_1 V_z)^2 \quad (44)$$

$$V_4^2 = (V_y \text{ Cos } a - V_x \text{ Sin } a)^2 + (h_2 V_z)^2 \quad (45)$$

where,

V_1 and V_2 = Effective velocities with cross on y-z plane

V_3 and V_4 = Effective velocities with cross on x-y plane

h = Sensor constant

a = Sensor angle with respect to the velocity component

When the thermal anemometry is used in a turbulent medium, the measured velocities also record the fluctuating portion of the components of the velocity vector in each direction. the elimination of the influence of the fluctuating component may be accomplished by setting the response time of the sensors to a relatively large value and carefully averaging the electrical signal produced. The averaging process used was to wait until the third decimal place of the indicated voltage was stabilized (approximately 45 sec.) and then average the last digit over 15 seconds. This procedure was adhered to throughout the experiments.

Experimental Results and Discussion:

The magnitudes of the total velocity vector for a circular orifice as determined by measurements carried out in the

experiments described above in comparison to calculated values is presented in figures A1 to A12 of Appendix 1. The solid line drawn in each figure represents the exact agreement between the theory and the experimental values. The results shown suggest that the agreement between the prediction by the approximate theory for the total velocity and the experimental measurements are good.

The results of the verification of all components for all shapes are summarized in Table 2. In this table, the summary is shown as the bias (percent mean difference) between the theoretical and experimental results with the theoretical values are taken as the points of comparison and the standard deviation of the differences. Even though the components of the velocity vector shows considerable scatter as signified by the standard deviations shown, the agreement between the theoretically and the experimentally obtained values is satisfactory. The larger scatter is observed in the magnitude of the components of the vector velocity. This is an understandable experimental phenomenon. As one can see from the anemometer equations above, the alignment and the angular placement of the probe are critical due to the ill-conditioned set of the anemometer equations, i.e. four equations will exist for three unknowns when the approach angle is 45 degrees exactly for two components and if the alignment is in correct, there will be five unknowns with four equations. In the probe design, the sensor angle is intentionally set at 45 degrees to the plane orthogonal to the cross in order

Table 2

Summary of Comparison Between Measured and Calculated Velocity Components for the three Shapes Studied

Shape		Average Percent Error for the velocity Component			
		Total	X	Y	Z
Circle	Bias	6.5	-12.6	14.1	18.2
	St. Dev.	9.2	14.2	11.4	11.7
Triangle	Bias	18.7	-22.4	32.1	40.2
	St. Dev.	22.4	20.6	17.7	28.0
Triangle (mod)	Bias	8.8	-16.0	13.8	13.8
	St. Dev.	12.8	13.1	13.4	13.4
Rhombus	Bias	14.2	-17.7	18.1	25.4
	St. Dev.	11.8	22.0	14.6	14.6
Rhombus (mod)	Bias	11.8	-15.6	21.3	21.3
	St. Dev.	10.6	20.3	12.6	12.6

Modified triangle and rhombus refers to the shapes with sharp corners rounded.

to maximize the response of velocity components in this plane and minimize the effect of film supports on the measurements. The compromise solution to this problem is to seek solutions of the equations above with an estimated total velocity angle. This procedure results in the loss of accuracy of the components, which is counterbalanced by the accuracy of the total velocity measurement as a result of compensating errors. This is apparent in Table 2, the scatter in the magnitude of the total velocity is about 10 percent in contrast to about twice that value in the components. This would suggest that a significant uncertainty is associated with the angle of the velocity vector, while its amplitude is well estimated. This observation is similar to the results obtained by Flynn and Ellenbecker(1987).

The bias and the scatter of the results pertaining to the triangular orifice was the largest and the same parameters for the results pertaining to the circular orifice was the smallest. The reason for this seems to be the failure of the theory in the close vicinity of acute angles of the triangle and the rhombus. In fact, when the results obtained from these specific areas in the triangular and rhombic orifice trials, the test results for the three orifices are very close. This observation is probably due to the poor distribution of face velocity near sharp corners due to the effects of the viscous forces. Since the theory assumes uniform velocity distribution at the orifice surface, large deviation from this assumption at severe corners probably influences the experimental outcome more drastically than the

open areas of the shapes.

With the empirical confirmation of the theoretically developed equations, the important question to raise is the method of application of results obtained. Obviously, for a rotationally symmetric circular orifice, both the experimental and theoretical results are reduced to a two dimensional representation. However, orifices with other shapes do not present this opportunity. For refined calculations where the representation of the velocity vector is important, the theoretical equations are reasonably simple to evaluate but for general design purposes, point by point evaluation of the velocity vectors is cumbersome and requires computer use. Although there is no simple way to circumvent this problem, the programing requirements for the calculations are simple and can adapted to use with a rudimentary micro computer.

B) Air Flow Generated by Flanged Suction Hoods with Adjacent Planes:

Recent theoretical and experimental studies which deal with freely suspended hoods (Esmen et al. 1986; Esmen et al. 1990 Flynn and Ellenbecker, 1985; 1986; 1987) made important advances in understanding the structure of the flow field in front of a hood. These studies showed that the theoretically developed equations could predict the flow field with sufficient accuracy, to allow their use in the design of hoods to increase both the capture and mechanical efficiency. The theoretical developments

reported in the papers cited above, one way or another depend upon the use of potential flow equations. The technique used by Flynn and Ellenbecker (1985) was the solution of the potential flow equation with a super imposed semi-empirical correction factor which resulted in simple equations for circular hoods. Unfortunately their method was not readily generalized to other shapes. ESMEN et al. (1986) used a point sink super imposition technique which can be generalized to arbitrary shapes; even though, this approach resulted in complicated equations for freely suspended hoods.

The original consideration of how an adjacent plane influences the centerline velocity of the flow field in front of a capture hood is due to Fletcher and Johnson (1982). Their investigation showed that if a hood would be placed on a table, the centerline velocity of the generated flow field would be increased significantly. Their results also showed the dependence of this increase on both the hood orifice shape and on whether an oblong hood were placed with the long side or the short side adjacent to the flanking plane. ESMEN et al. (1986) extended theoretical calculation of the velocity field generated by a flanged oblong orifice hood to include one flanking plane perpendicular to the hood plane. Such an extension of the theoretical work, albeit limited, covered a number of industrial situations where hoods are placed on tables. Their method of two point sink representation of iso-kinetic lines of the flow field in front of a hood depends upon the construction of two virtual

sinks on the orifice surface one located at the geometric center of the opening and the other at the point corresponding to the minimum distance between a point under consideration on the iso-kinetic surface (ESMEN et al. 1986). This approach presents no conceptual difficulties if no obstruction is present between a point in space and the surface of the opening. This earlier paper considered the truncation of the geometric surface by an adjacent plane as a solution to remove the problem created by the adjacent plane. This approach was acceptable at locations sufficiently far from the adjacent plane with respect to the direction of the velocity vector and reasonably accurate for the norm of the vector (magnitude of the velocity) in the entire flow field. However, if the adjacent plane is at an angle, the solutions obtained by truncation do not give realistic answers and truncation of the flow field is theoretically awkward as there is no reason to accept the truncation of the flow field as a theoretically justifiable solution. In reality, the adjacent plane does not truncate the flow field but rather distorts it. Heuristic considerations based on the distortion of the flow field are considered in this paper as an extension of the flow field equations to the cases which involve adjacent planes.

Theoretical Considerations

The extension of equations describing a flow field generated by an orifice to cases which involve adjacent planes requires a brief discussion of the governing equations of flow between two

boundaries at an angle to each other. In order to keep the cumbersome mathematical details to a minimum, the consideration of two dimensional potential flow can be used without the loss of generality. In these cases, the stream function F(z) of the complex variable z is expressed in the general form (Prandtl and Tietjens;1957):

$$F(z) = \frac{C}{n} z^{n} \qquad (46)$$

where,

C = Constant

n = Constant which describes the angle between the planes

In this function n = 1 corresponds to the motion along the real axis; $1 < n < 2$ corresponds to the motion with an obtuse angle between the planes; n = 2 corresponds to the motion with a right angle between the planes and finally $n > 2$ corresponds to motion with an acute angle between the planes. Consider an adjacent plane which intersects the hood plane at a distance L from the orifice center at an arbitrary angle Θ as shown in figure 5. On the basis of dimensionless variables with respect to the orifice size: $h = x/W$, $g = (L-y)/W$ it may be shown that the components of the velocity vector are:

$$V_x(n) = V(1)\, R^{n-2} \quad (g \sin n\phi + h \cos n\phi) \qquad (47)$$

$$V_y(n) = V(1)\, R^{n-2} \quad (h \sin n\phi - g \cos n\phi) \qquad (49)$$

where the co ordinate system is as shown in Figure 5 and

$$R^2 = h^2 + g^2 \qquad (50)$$

$$n = 1 + \tan(\theta/2) \qquad (51)$$

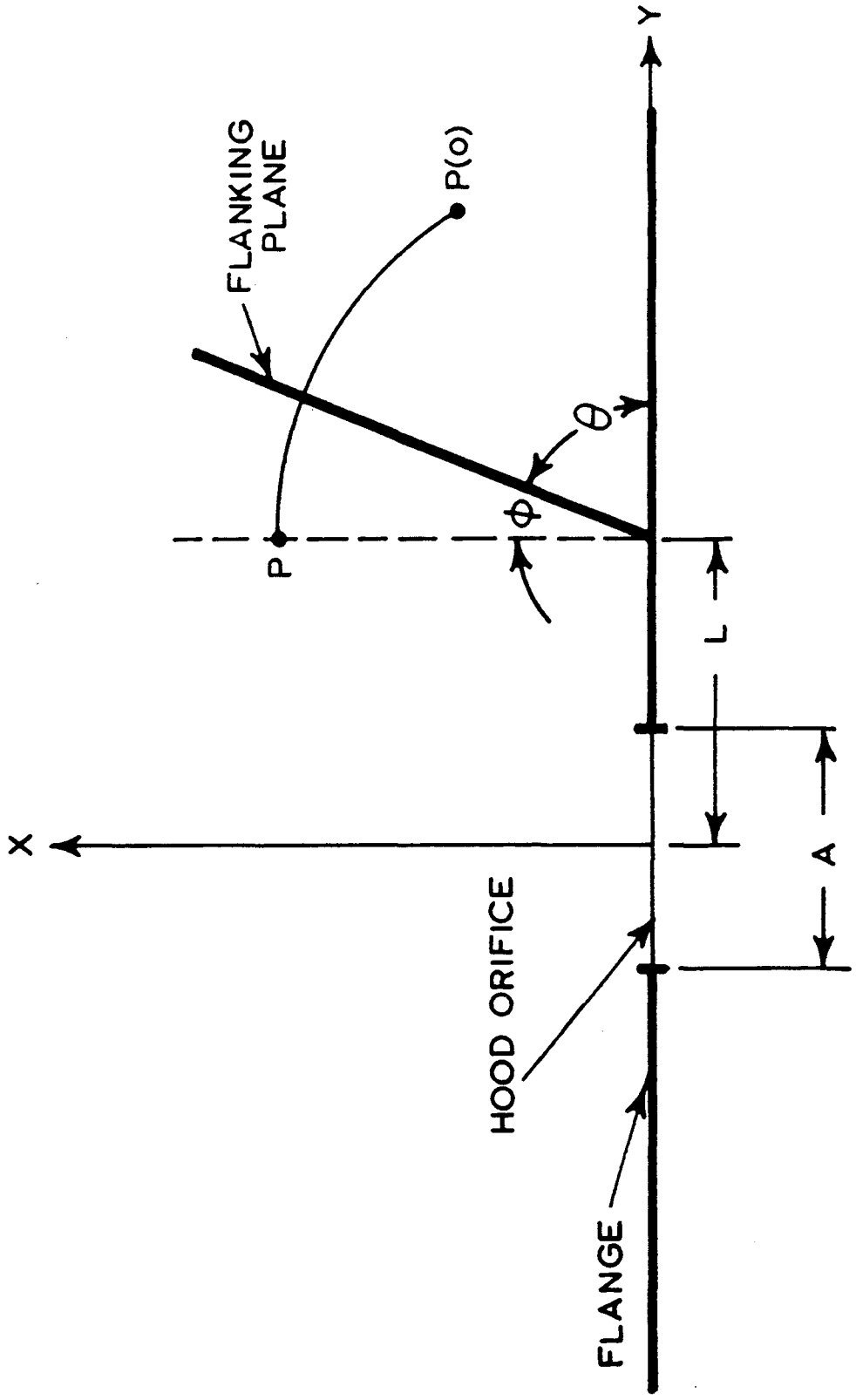

Figure 5. The schematic description of the parameters used in the transformation equations.

The direct application of these equations to the flow field generated by a sink presents a number of mathematical problems. The most obvious one is that the stream function which describes the flow field due to the presence of the corner is most conveniently expressed when the center of the co-ordinate system is translated to a point on the intersection of the hood plane and the adjacent plane. Unfortunately, such a translation, makes the solution of the equations which describe the flow induced by the orifice intractable. This dilemma may be solved by investigating the effect of the corner on uniform flow as expressed by the equations above and finding the proper function to show this effect on the flow field generated by the orifice. Algebraic manipulation of equations 46 and 47 shows that in a flow field with a uniform velocity upstream of the corner, the presence of a corner deforms the domain of the flow field onto another domain by a homogenous continuous deformation in which the norm is preserved. In simpler terms, under the mathematical transformation, the magnitude of the vector is preserved but its direction changes. Heuristically this observation may be utilized to deform the flow field generated by the hood orifice.

Consider an adjacent plane which intersects the hood plane at L with an arbitrary angle Θ as shown in Figure 5. If this plane is removed by rotation such that $\Theta = 0$, then the point $P(\Theta)$ corresponds to point P(0). Note that the flow field equations satisfy both the mass balance and the boundary conditions (ESMEN et al. 1986). Thus, if the functions which define the vector

velocities generated by the hood orifice without an adjacent plane (free hood) are mapped unto the space defined by the truncation of the flow field by the adjacent plane, then the mass balance and boundary conditions will also be satisfied. This mapping is readily accomplished by the radial vector used in the description of the flow within the corner and a conveniently scaled angle of rotation . The properties of the mapping function are such that the when $\theta=0$, the components of the velocity in the transformed flow field approach the total flow field value and as Ω approaches $\pi/2$, the contribution of the rotated flow field vanishes. This relationship may be described by:

$$V_x(P(\Omega))=k\left[(V_y(P(0))\sin\theta + V_x(P(0))\cos\theta)\sin\Omega + V_x(P(\theta))\right] \quad (52)$$

$$V_y(P(\Omega)) =k\left[(V_y(P(0))\cos\theta + V_x(P(0))\sin\theta)\sin\Omega + V_y(P(\theta))\right] \quad (53)$$

$$V_z(P(\Omega)) =k\left[V_z(P(0))\sin\Omega + V_z(P(\theta)\right] \quad (54)$$

with,

$$P(0) = (x\cos\theta + (L-y)\sin\theta,\ x\sin\theta -(L-y)\cos\theta + L, z) \quad (55)$$

and,

$$\Omega = \frac{\pi}{2(\pi-\theta)}\left[\frac{\pi}{2} - \arctan\left[\frac{(L-y)}{x}\right]\right] \quad (56)$$

Thus the magnitude of the vector becomes:

$$\| V(P(\Omega)) \|^{1/2} = \left[V_x(P(\Omega))^2 + V_y(P(\Omega))^2 + V_z(P(\Omega))^2 \right]^{1/2} \quad (57)$$

For the evaluation of equations 52 to 57, the value of k must be known. We note that the velocity $V(P(\theta))$ satisfies the mass balance,and therefore the ratio of the magnitudes of $V(P(\theta)$

and $V(P(\Omega))$ evaluated with k = 1 may be used to define the scaling factor. consequently,

$$k = n \, \| V(P(\Theta)) \|^{1/2} / \| V(P(\Omega), k=1) \|^{1/2} \quad (58)$$

The directional vector may be calculated by:

$$D = (V_x(P(\Omega)) \, e_x + V_y(P(\Omega)) \, e_y + V_z(P(\Omega)) \, e_z \,) / \| V(P(\Omega)) \|^{1/2} \quad (59)$$

The vector velocities required in the flow field generated by the free hood may be calculated by any appropriate set of equations which describe the flow vectorially. In this work, the velocity equations developed by the authors (ESMEN et al.; 1988) were used, primarily because they express the velocities in a Cartesian co-ordinate system and can be used in the calculations without a co-ordinate transformation. In addition, all of the computer programs used in the calculations were readily available in our laboratory.

The verification of the theoretical results in their simplest form may be accomplished with the data available in the literature. Fletcher and Johnson (1982) measured centerline velocities of unflanged hoods with seven different aspect ratios placed on a table with the long side and the short side next to the adjacent plane. In the theoretical prediction the equations above were utilized in conjunction with a modification of the velocity field equations for an unflanged hood with an oblong orifice. The results of these calculations and the corresponding experimental results of Fletcher and Johnson are shown in Figure 6. The agreement between the theoretical and experimental values is excellent.

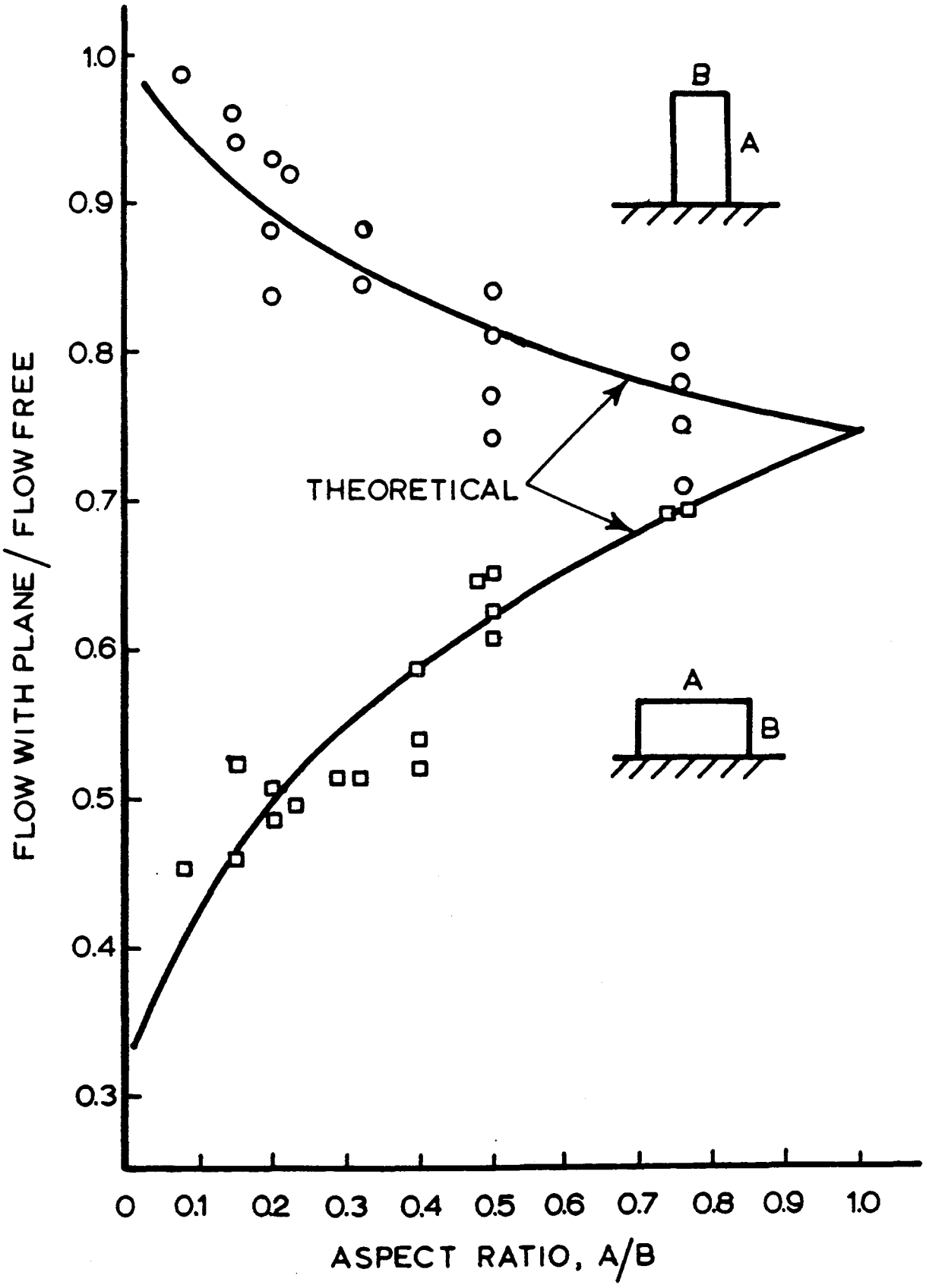

Figure 6. The comparison of theoretically obtained results with the results reported by Fletcher and Johnson (1982)

Since the main utility of the theoretical development is the full description of the flow field in the presence of one or two adjacent planes at arbitrary angles and arbitrary locations, then it is necessary to generalize the equations given above. This can be done by sequential application of the mapping functions. In order to show the sequential application clearly, consider the following four cases shown in Figure 7 which exhaust all possibilities. In each of these cases it will be understood that each adjacent plane shown is at an arbitrary but specified angle with respect to the hood plane and the location of an adjacent plane is specified by the intersection of the adjacent and hood planes (the baseline). In the first case, one adjacent plane is located such that the baseline is perpendicular to one of the natural axes of the orifice. This is the direct application of the equations above and the velocities of the free hood (primary values) are transformed to give the final velocities (transformed values). In the second case, another adjacent plane is added to the first case with the two baselines perpendicular. In this case, the transformed values due to one adjacent plane are treated as the primary values for the calculations of the effects of the second adjacent plane. In the third case, two adjacent planes with perpendicular baselines are at an arbitrary but specified angle with respect to the natural axes of the hood orifice. In this case, the primary values are rotated to set the co-ordinate system to conform to the second case. This can be achieved readily by simple trigonometric relationships that exist

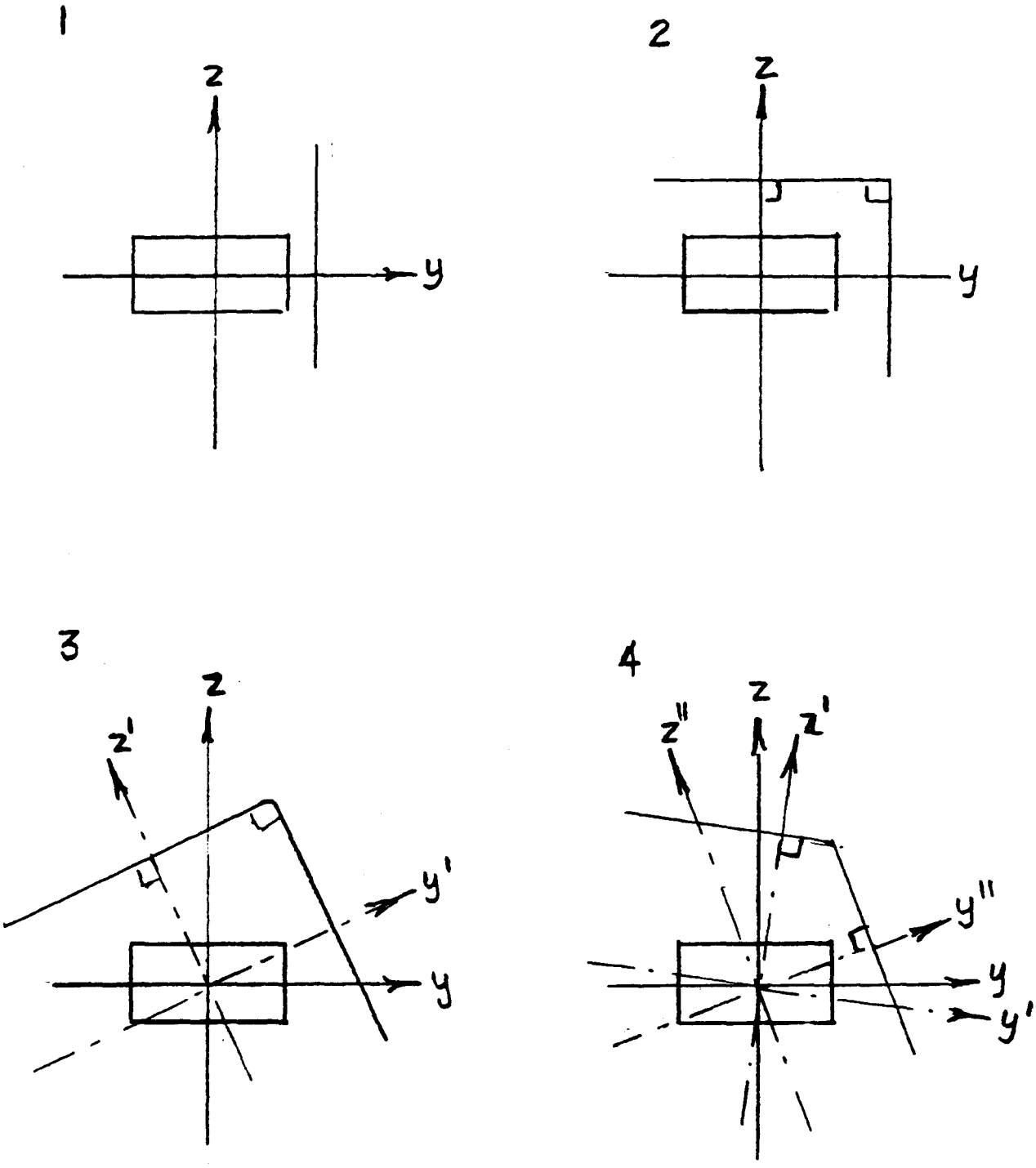

Figure 7. Schematic representation of adjacent plane locations may be addressed by the theoretical development.

between the natural and the rotated axes. The last case is the direct generalization of the third case. Although the computer calculation procedure for each case is straight forward, the mathematical transcriptions of the transformations are cumbersome and consequently they are not given.

Experimental Investigation

The simplest shape of an orifice which can be studied is a circular orifice. In the experimental investigation of the influence of adjacent planes on the flow field generated by the suction of the hood, a hood with a circular orifice of 5 cm radius was used. The velocity measurements of the flow field generated by the hood suction were made with an X probe hot film anemometer as descibed above.

In the experimental system used, one adjacent plane was stationary, at 90 degrees to the hood plane and located 11.4 cm from the center of the orifice. The other adjacent plane was perpendicular to the fixed plane, but both its location and its angle with the hood plane were varied. Consequently, 3 configurations were readily obtained for the experimental verification of the theoretical development above.

The comparison of theoretical values of air speed calculated to the experimentally measured values are shown in figure 8. The results shown in these figures indicate that the agreement between the theory and the experiments is satisfactory.

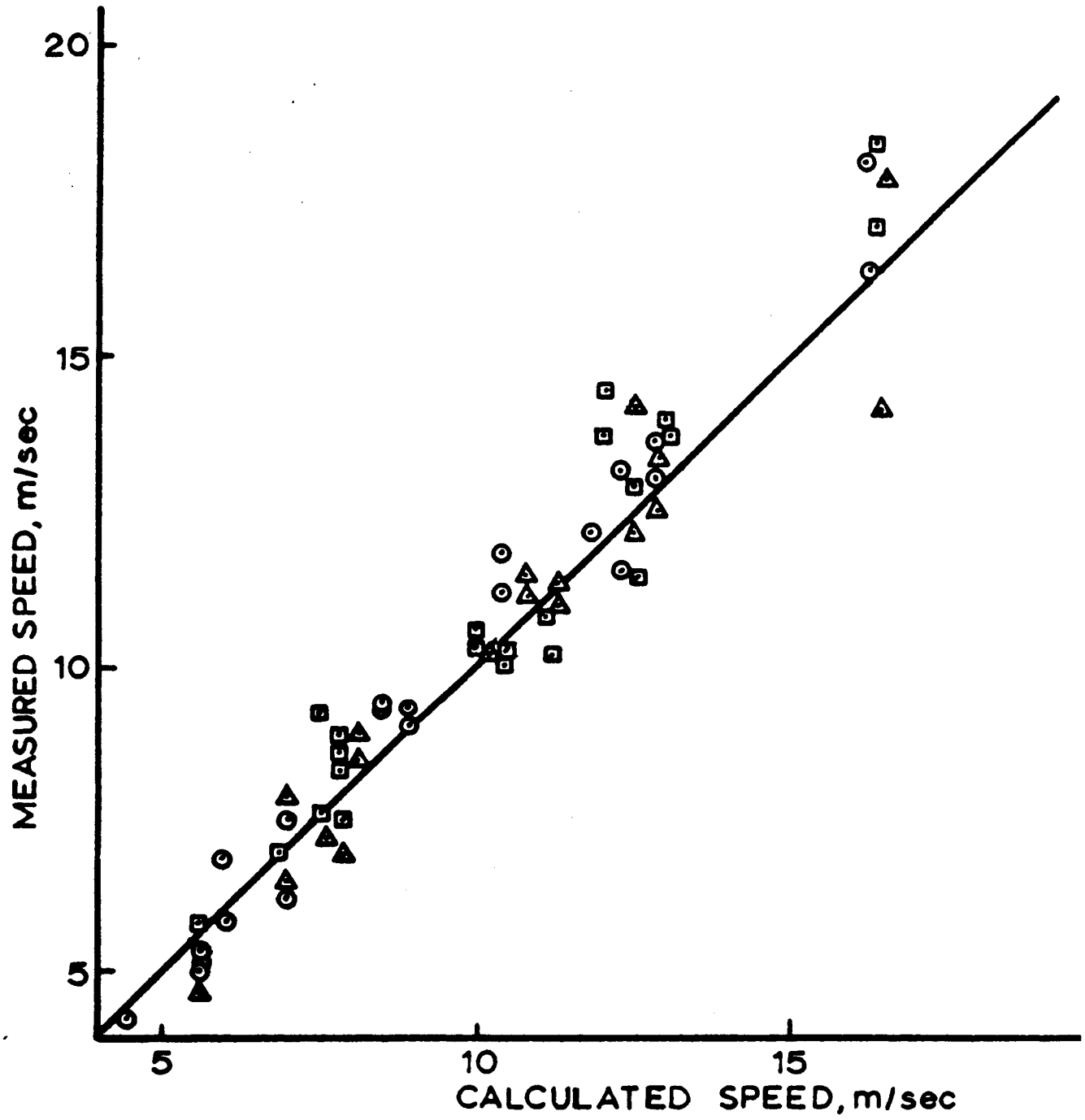

Figure 8. Comparison of calculated and measured air speeds for the three cases experimentally studied.

Discussion of Results

Admittedly, the basic exterior hood design in the presence of adjacent planes could be satisfactorily carried out using the results reported by Fletcher and Johnson (1982). The availability of a theoretical formulation of the influence of adjacent planes on the flow field generated by a hood is important for several other reasons. The ability to predict the entire velocity vector field enhances the estimation of the effects of interferences such as drafts.

In addition, the possibly more important application of the theory developed is in the consideration of the effects of obstructions placed in front of a hood on the velocity field generated by the hood. In general, a hood normally operates in conjunction with a process and the physical size of the process placed in the flow field is bound to interfere with the hood operation. Intuitively, this interference is expected to be detrimental to the hood operation. However, it is possible to imagine cases in which the physical size of the process may enhance the capture of contaminants by the hood. If the process can be viewed as a number of adjacent planes placed in the flow field, then the theoretical development presented here is a promising starting point for further development. In such an endeavour, theoretical consideration of the effect of finite adjacent planes on the flow field would be required. Also,the complete solution of the flow field equations with an obstruction is expected to be more complicated due to the wake effect. Even

with these limitations, if the theoretical approach presented in this section can be extended to the estimation of the influences which result from simpler obstruction geometries, it would be promising as a starting point for further theoretical development in the consideration of obstructions in the flow fields generated by hoods.

C) Optimization of Freely Suspended Exterior Hoods in Industrial Ventilation

In the design of an exterior hood, the value of the airflow rate through the hood can be found if specification of the "reach" of the hood is given. By the reach of the hood we mean a set of air speeds induced by the hood, to be achieved or exceeded at specified locations in front of the hood. If the velocity profile generated by the hood air flow is know, the problem is simply matching the velocity profile with the specifications to obtain the flow rate which will achieve the correct air speeds. There are a number of expressions which give velocity profiles with about equivalent accuracy. Thus, any one of these expressions can be used to design a hood. Clearly, if the air speed specifications are given correctly, then the capture efficiency of the hood is expected to be optimal. It must be noted that the optimum for the capture efficiency can be made independent of cross currents, because the effect of cross currents can be included into the specification of the air speed. This seemingly direct and simple method of computation, which

determines the minimum flow rate to accomplish the desired result, is flawed with respect to the mechanical efficiency of the hood. This flaw is due to the a priori selection of the hood geometry and orifice size without a quantitative investigation of the possibilities of achieving the same end result with a hood of different geometry and/or orifice size. Although the experience of the designer may be invoked as an influencing factor in the design, even for an experienced designer it is unlikely that the consequences of such alternatives have ever been a consideration.

In order to simplify the theoretical development, it will be assumed that a specific value of air speed on all points of a regular geometric shape defined on a plane located in front of a hood is given as the design criterion for the hood. It is important to note that the restriction of specification surface to a plane rather than a curved surface will not give a general solution. Therefore, it may be considered to be a limitation of the theoretical development. However, such a specification would be sufficiently common in the industrial applications and more importantly, the methodological approach can be presented without undue complexity of the mathematical formulation so that the results would be useful to a ventilation system designer.

Theoretical Considerations

In the investigation of the implications of hood orifice geometry and in the selection of proper size of the orifice, the

development of the theory is facilitated if the specification geometry is chosen in a way that the distances measured from the point on the hood is readily accomplished. This will suggest that the shape of the specification surface is symmetric with respect to both of the axes of the plane. An oblong or a circle would satisfy this criterion. Since a square has four extremal points, then the structuring of the optimization problem can be reduced to matching the air speed generated by the hood to the specified air speed at the extrema. This process would be sufficiently general, in the sense that the specification can be in terms of a component of a vector.

Suppose it is necessary to generate air speed of V_C at the surface of an oblong located on a plane parallel to the hood surface and centered on the x- axis with its sides parallel to the xz and yz planes. Furthermore, suppose that it is necessary to keep the hood face velocity equal to or below a specified value V_0 . Let A and B be the maxima of the y and z coordinates respectively. For an oblong hood, with sides a fraction c of A and B placed with its center at the origin (Figure 9) minimization of the flow rate Q might be sought by the object function:

$$Q = L^2 \, f(a,b,h) \, V_C \tag{60}$$

Subject to:

$$V_C \, f(a,b,h) / \, 4abc^2 \; < V_0 \tag{61}$$

where,

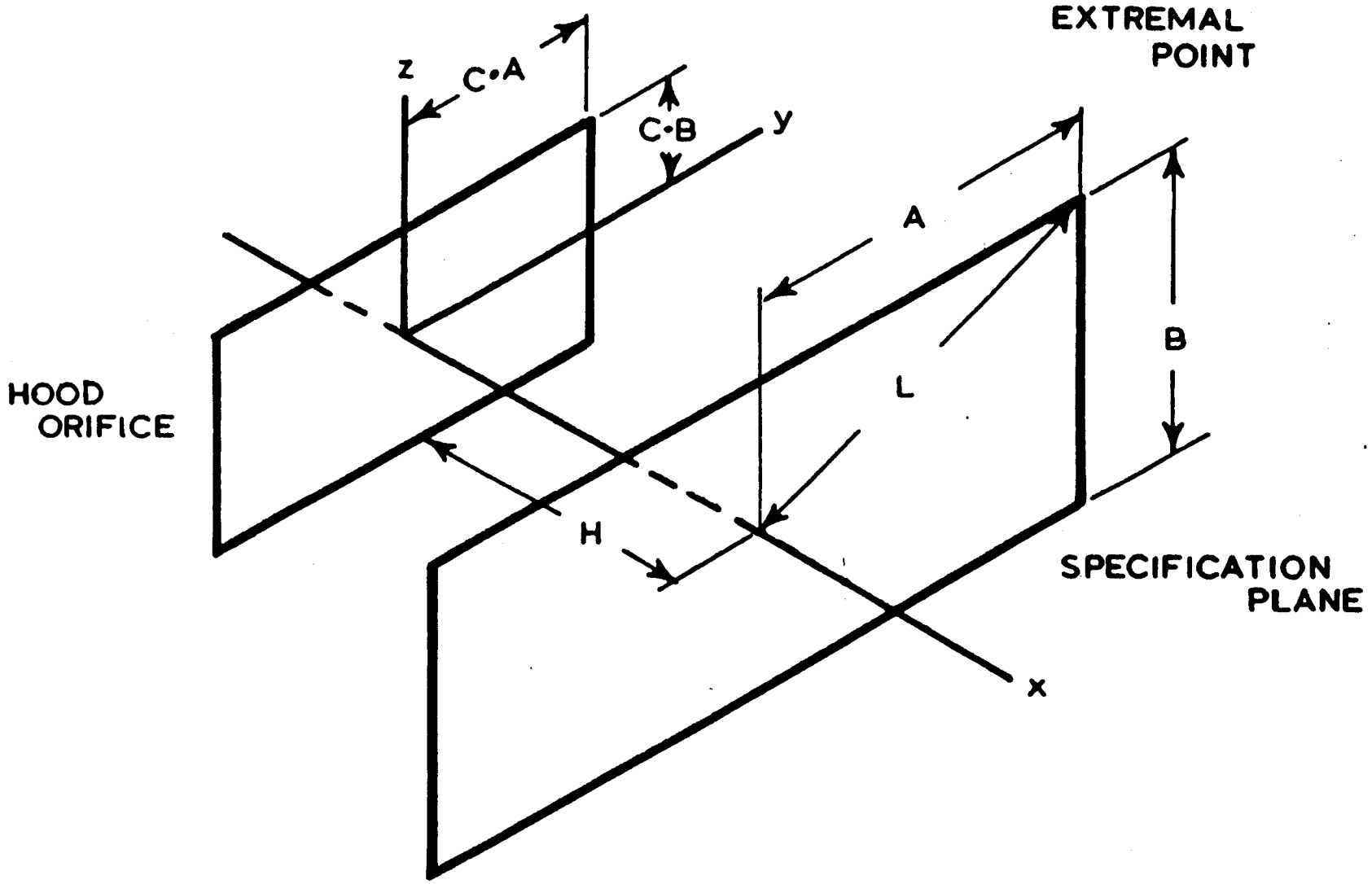

Figure 9. The parameters and the Configuration used in the derivation of hood optimization

a = Dimensionless specification oblong side, A/L

b = Dimensionless specification oblong side, B/L

h = Dimensionless distance to the specification surface,H/L

For an oblong orifice, the function f(a,b,h) may be shown to be represented by the non-dimensionalized velocity scaling function (Eq. 60) multiplied by the hood orifice area:

$$f(a,b,c,h) = \pi(a+b)cr + 2\pi r^2 + 4abc(c + h(a+b)/(a^2 + b^2))^{1/2} \quad (62)$$

with,

$$r^2 = h^2 + (1 - c)^2 \quad (63)$$

Equations 60 through 63 can be extended directly to a circular orifice by taking c.L to be the radius of the orifice. In such an extension, Equations 61 and 62 will have to be modified to conform to the description of the flow field in front of a circular orifice. The modified equation for a circular orifice hood may be shown to be :

$$f_C(a,b,c,h) = \pi^2(c\,r + r^2)/2 + \pi\, c\,(c^2 + K\,h^2)^{1/2} \quad (64)$$

$$K = 4/(\pi^2 - 2\pi)$$

and,

$$V_C\, f(a,b,h)/\pi(a^2 + b^2)c^2 < V_0 \quad (65)$$

The minima sought may be found directly by differentiating either equation 62 or equation 65 with respect to c and finding the root of the resulting equation which is between zero and one. For an oblong orifice, the non linear equation to be solved is:

$$\pi(a+b)\,\frac{h^2+1-3c+2c^2}{(h^2+1-2c+c^2)^{1/2}} + 4\pi(c-1) + 4abc\,\frac{2c^2+h(a+b)}{(c^2+h(a+b))^{1/2}} = 0 \quad (66)$$

and similarly for a circular orifice:

$$\frac{\pi}{2} \cdot \frac{h^2+1-3c+2c^2}{(h^2+1-2c+c^2)^{1/2}} + \pi(c-1) + \frac{2c^2+K\,h}{(c^2+K\,h)^{1/2}} = 0 \qquad (67)$$

If the specification surface, instead of an oblong, is a circular one then calculation process may be modified by taking two different values for square or circular hoods. It may be shown that for a square orifice hood the square hood A = B and L = A$\sqrt{2}$ and for a circular orifice hood L = A. With these altered specifications equations 60 through 67 apply to optimization without further change.

In general,the process of calculation is straight forward and with the use of a computer presents no significant problems. However, in certain cases no root may exist in the zero to one interval. This suggests that the global optimum design does not exist for that condition. This situation will arise when the dimensionless frontal distance h is sufficiently large. Consequently, the local optimum which is defined by the maximum face velocity specified in equation 61 or 66 and the corresponding orifice size may be used.

For infrequent design problems where the use of computer is not warranted or for those who does not have a ready access to a computer, there a number of simplifications, albeit limited, reduce the calculations to simple use of tables. To develope these simplifications, consider the specification surface to be bounded by a square, i.e. the sides are such that A = B. then the optimization can be carried out utilizing the

values shown in Table 3. The simplest use of this table may be illustrated by an example. Suppose the specification surface is located 10 cm from the hood plane with A = 0.25 m. If the air speed desired on this surface is 1 m/sec and the maximum face velocity allowed is 25 m/sec then the optimum hood size for a square hood is calculated as follows:

L = A^1/2 = 0.35355 thus h = H/L = 0.283. Therefore, interpolating the proper values from Table 3, f(h) = 3.6191 and c = 0.784; consequently, the optimum value of the side of the square hood is 19.6 cm and from equation 60 the a volumetric flow rate is 0.45 m^3/sec. Similarly, for a circular hood, the optimum radius is 22.5 cm and the flow rate is 0.49 m^3 /sec. Thus for this simple illustration, a square orifice hood would be an optimum choice.

If the example above is recalculated using a circular specification, the optimum square hood would be the same, but the optimum circular hood would have L = 0.25, h =0.40 which results in a hood radius of 13.0 cm and flow rate of 0.31 m^3/sec. In this case a circular hood would be superior.

It is important to note that the theoretical results developed above are not inherently limited to applications which involve specification surfaces assumed in the development. Obviously, if the specification surface is not nearly a square circular or square orifice hoods will be inherently inappropriate but must be replaced by oblong orifice hoods. Finding the roots of the derivative of the objective function may be carried out by

TABLE 3.

Optimization Parameters for Squares and Circles

Dimensionless	Square		Circle	
Distance	C	f(a,h)	C	f(a,h)
0.05	0.9351	2.2007	0.7734	3.1161
0.10	0.8926	2.4464	0.7344	3.2874
0.15	0.8594	2.7265	0.6953	3.4966
0.20	0.8291	3.0372	0.6641	3.7355
0.25	0.8018	3.3768	0.6211	3.9989
0.30	0.7754	3.7440	0.5859	4.2843
0.35	0.7598	4.1381	0.5508	4.5893
0.40	0.7266	4.5588	0.5156	4.9126
0.45	0.6992	5.0057	0.4805	5.2530
0.50	0.6758	5.4785	0.4414	5.6094
0.55	0.6562	5.9770	0.4062	5.9811
0.60	0.6328	6.5012	0.3672	6.3672
0.65	0.6104	7.0511	0.3203	6.7667
0.70	0.5869	7.6263	0.2634	7.1790
0.75	0.5635	8.2270	0.2266	7.6030
0.80	0.5400	8.8531	0.1719	8.0375
0.85	0.5166	9.5044	0.1094	8.4809
0.90	0.4932	10.1810	0.0312	8.9307
0.95	0.4688	10.8828	------	------
1.00	0.4434	11.6098	------	------
1.05	0.4209	12.3619	------	------
1.10	0.3965	13.1391	------	------
1.15	0.3721	13.9414	------	------
1.20	0.3467	14.7688	------	------
1.25	0.3203	15.6211	------	------
1.30	0.2949	16.4984	------	------
1.35	0.2695	17.4007	------	------
1.40	0.2441	18.3278	------	------
1.45	0.2148	19.2799	------	------
1.50	0.1914	20.2567	------	------

Circular orifices with maximum face velocity:

$$L^2 f_c(a,b,h) V_c - \pi (a^2 + b^2) c V_0 = 0$$

Oblong orifices with maximum face velocity:

$$L^2 f(a,b,h) V_c - 4 abc^2 V_0 = 0$$

hand but such a calculation would be cumbersome. Although the computerized solution is simple, when a computer is not available, the optimization of each dimension of the orifice may be carried out approximately,one at a time by treating each side as an independent imaginary square hood. Although the orifice dimensions determined in this manner may not predict the exact optimum design values, the resulting dimensions are expected to be near the optimum values. The flow rate for such an orifice can not be calculated directly from Equations 60 to 63.

Experimental Results:

The direct experimental verification of the optimization procedure given above is at best cumbersome. Such an experiment would involve the construction of a very large number of hoods. However, an indirect experimental verification of the procedure may be accomplished by showing that a few representative hoods may be constructed and studied. In the experimental study carried out to verify the theoretical calculations indirectly, three oblong hoods were constructed. These hoods were 5 cm. by 5 cm. square, 3 cm. by 5 cm. oblong and 4 cm. by 8 cm. oblong. With hood opening fixed, conditions under which these hoods will be optimum were calculated for different values of frontal distance and for each condition, the optimum flow rate was predicted. The air speed was measured at each the theoretically determined specification point and the flow rate was adjusted until the air speed specification is fulfilled. This experimentally determined

flow rate was then compared to the theoretical flow rate. All air flow and air speed measurements were carried out by hot wire anemometry. The hood airflow measurement was carried out by measuring the air speed by a traverse as close to the orifice plane as possible.

The comparison of the calculated optimum and the measured flow rates are given in figure 10. The results suggest that the optimization procedure is satisfactory and perhaps slightly pessimistic in the indication of the flow rate required. On the average, about 10 percent less flow was required than it was calculated as necessary.

Design Applications and Discussion

The application of the results presented above to the design of freely suspended hoods with single square, circular or oblong orifices is a straight forward process but it must be recognized that the success of the hood design based on such calculations will ultimately depend upon the correct specification of the velocities to be generated at specific locations. The estimation of these velocities is beyond the scope of this paper and may be found in manuals dealing with currently accepted practice. If the specification surface is judged to be a curved surface rather than a plane or if the vector components of the velocity at specified points are sought, new objective functions following the theoretical development above can be found. Alternately, the hood size may be selected at an extremal point by considering

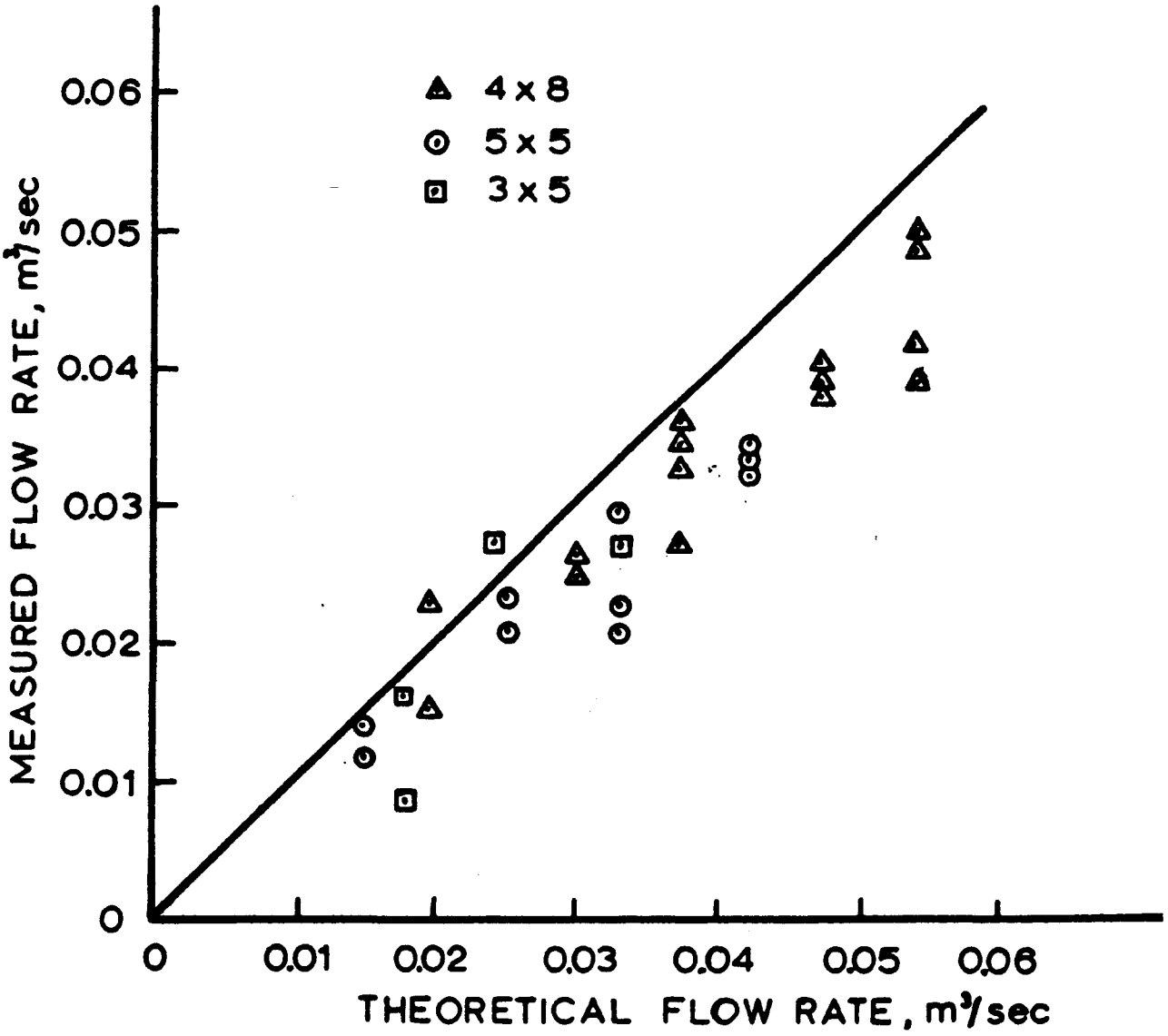

Figure 10. Comparison of Theoretically and experimentally obtained flow rates for three hoods.

that point to be one of the vertices of an oblong specification surface and the proper flow rate through the system can be calculated by point matching between the generated flow field and the required flow field.

In order to show the efficacy of the optimization procedure developed here, five hypothetical cases were compared to the traditional design procedure. The results of this comparison are shown in Table 4. For the cases shown in Table 4, the efficiency gain through optimization is about 13 percent with a range from 2 to 30 percent. These cases were not constructed with a forethought to show the effectiveness of the optimization procedure, but rather they were arbitrarily selected. Since the optimization process is based on the velocity profile in front of the hood, and the traditional design procedure which is based on the adjustment of the centerline velocity of the hood, then the hood designed by the optimization procedure ensures that the air speeds specified on the specification plane are satisfied. On the other hand such a statement would not necessarily be correct for the design based on centerline velocity. Consequently, the hoods designed through the process described above would always have a superior total efficiency as compared to the traditionally designed hoods.

TABLE 4.

Comparison of Traditional and Optimized Designs

(unit control speed)

Design	B vert. cm	A Hor. cm	H cm	Diameter or Height cm	Width cm	Flow m^3/sec
CASE I	15	15	15			
Traditional Square				30	-	0.354
Optimum Square				27	-	0.254
CASE II	20	30	25			
Traditional Oblong				40	60	1.12
Optimum Oblong				33	49	1.01
CASE III	10	20	30			
Traditional Oblong				20	40	0.902
Optimum Oblong				12	24	0.880
CASE IV	20	20	25			
Traditional Square				40	-	0.889
Optimum Square				25	-	0.830
CASE V	20	20	10			
Traditional Square				40	-	0.421
Optimum Square				19	-	0.358
Circle				15	-	0.359

D. The Effect of Turbulence on Exhaust Hood Capture Efficiency:

The use of mechanical ventilation systems of one type or another is a common practice in industry. These ventilation systems are used to control heat, odor, and exposure to potentially toxic airborne material. Ventilation systems are characterized by two general types, namely, general ventilation and local exhaust ventilation. In general ventilation, the occupied space is ventilated by means of introducing clean air. In local exhaust ventilation, the contaminated air is extracted at convenient points close to each source of contamination and clean air is supplied to the room to make up for the amount of air extracted. In contaminant control, the most effective use of exhaust ventilation is a local exhaust system. It must be noted that a local exhaust ventilation system also acts as a general ventilation system. While different types of exhaust ventilation systems can be found in almost any setting from the laboratory to the industrial workroom, the essential feature of all such systems is an opening through which an appropriate amount of air is drawn.

The most commonly used reference in exhaust ventilation design today is "Industrial Ventilation: A Manual of Recommended Practice" published by the American Conference of Governmental Industrial Hygienists. The manual presents equations for calculating the air flow in front of free hanging hoods of various geometries with or without flanges. The manual defines capture velocity as the velocity at any point in front of the

hood necessary to overcome opposing air currents and to capture the contaminated air by causing it to flow into the exhaust hood.

The equations used in the ventilation manual were derived primarily by Dallavalle some fifty years ago. The equations are simple, easily evaluated expressions owing largely to the fact that sophisticated analytical and computational instruments were not available at that time. To this end recent research has focused on characterizing the entire flow field in front of the hood. In the traditional and the more recent design considerations, the effects of cross drafts are considered as an idealized case where the control of the contaminant is strictly influenced by the perfect motion of the air. This approach is justifiable if the local mixing of the contaminant due to turbulent diffusion is negligible. If the mixing is predominantly due to molecular diffusion, then neglecting mixing would be sufficiently accurate to justify this simplification. However, mixing under turbulent air flow may cause significant dispersion of the pollutant before the contaminated air reaches the hood.

Theoretical considerations:

In any investigation the first thing that must be decided is what parameter is to be investigated and how it will be defined. For the purposes of this investigation, capture efficiency was defined as the ratio of the concentration of acetone vapor in the exhaust stream as measured with a vapor generator positioned at an experimental point, to the concentration of vapor in the

exhaust stream when the generator was positioned at a reference point. The reference point was chosen such that it was reasonably certain that all of the vapor generated at the reference point was captured by the hood at all times under all conditions.

In order to construct a mathematical model for the capture efficiency of a hood, we consider the two components of hood efficiency. Suppose the source is located sufficiently far away from the hood such that the hood acts solely as an entry point of a general ventilation system. In this case, the hood efficiency will be a minimum. Any increase in this efficiency due to the closer proximity of the source to the hood may be viewed as the capture efficiency of the hood. The capture efficiency of the hood is reduced by the amount of material dispersed due to mixing. The dispersion of the contaminant may be separated into three components based on the mechanism of dispersion. These components are, molecular diffusion, convective dispersion and turbulent diffusion. The turbulence generated by the action of the hood alone, molecular diffusion and convective dispersion would be present in the presence or absence of a superimposed turbulent stream. Consequently, at any given point, the effect of turbulent dispersion may be estimated by the change in capture efficiency in the presence of a superimposed turbulent stream.

The simplest way to model mixing would be to consider sufficiently small pockets of air to act as solids containing and not containing contaminant and to treat the mixing process as a

simple first order mixing process as observed in many stirred batch mixers. The probability of a small unmixed volume element, w, is related to the total volume, W, and time, t, by (Coulson and Mitra ;1950):

$$\text{Prob} = \exp\left[-\text{constant} \left[1 - \exp(-t) \right] w/W \right] \qquad (68)$$

As time approaches to infinity, the probability of the unmixed element approaches to:

$$\text{Prob} = \exp\left(-\text{constant}.\ w/W\right) \qquad (69)$$

If the ratio of these hypothetical volumes is related to the eddy size, then the ratio is expected to be a ratio of the dissipation energy of the two streams. The dissipation energy is measured by the ratio of the square of air speeds of the mixing streams, R, by a power, n, then the probability statement may be expressed as:

$$\text{Prob} = \exp\left[- k R^n \right] \qquad (70)$$

This probability is expected to act as the proportionality function between the efficiency of a hood with undisturbed, E_o ,and disturbed streams, E_d ; this relationship may be expressed as:

$$E_d = E_o \exp\left[- k R^n \right] \qquad (71)$$

In the region where the undisturbed efficiency of the hood is unity, the turbulent jet contribution to the deterioration of efficiency is simply the measured efficiency of the hood. As this system is viewed as the mixing of two turbulent jets (one jet created by the exhaust hood and the other a turbulent jet

superimposed), turbulence is produced by the dissipation of kinetic energy of the jets. Because, this is the only source of energy in the system as there is no external mechanical mixer or source of heat to provide energy to the system. The kinetic energy dissipation is related to power by the efficiency of turbulence production and the mass of the fluid. For constant efficiency between two different systems Corrsin (1964) developed an equation for scaling the power requirements between the systems :

$$P' = K_e \, K^3 \, K_s^2 \, P \qquad (72)$$

where, K_e depends on the geometry and relates the change in mass between the systems as a function of dimension, i.e. length, and K_s depends on the nature of the material. If K and K_s are approximately equal, then the scaling will vary as the 1/6 power of the ratio of P'/P. If Ks is the controlling factor then the scaling will vary as the 1/3 power of P'/P (Corrsin; 1964).

The scaling concept developed by Corrsin for mixers may be applied to this system. Consider the experiment as a series of mixers, each identical in all respects. Each is driven at a different power input (turbulence generating power) and the "mixing" is measured. By selecting the comparison points in a region where the efficiency is 1 when there is no superimposed cross draft, it may be claimed that the effect of mixing is negligible with P, and consequently the measured change in efficiency by the superimposition will be a result of the superimposed velocity gradient and turbulent mixing. The effect

of turbulent mixing may be enhanced by providing a grid in front of the superimposed stream to generate nearly isotropic turbulence.

Consideration must now be given to the geometry related constant K_e . This constant can be viewed as an attenuation constant. Figure 11 illustrates the relationship between the jet induced by the exhaust hood and the jet used to create the turbulence. When $\Theta = 0$, then the turbulent stream is in direct opposition to the exhaust stream and K_e is expected to assume a maximum value. When $\Theta = \pi$ the streams are acting in concordance and K_e is expected to assume a minimum value. For convenience, the expression for K_e is chosen to be:

$$K_e = K_0 \left[1 + K_1 \cos (\Theta / 2) \right] \qquad (73)$$

K_0 is a speed dependent and K_1 is a position dependent constant.

In a given experiment, if all the flow parameters are kept constant and the superimposed stream is oscillated with a regular period such that Θ changes $\pm \pi / 4$ from the normal to the hood stream, the average K_e may be expressed as:

$$K_e = K_0 (1 + 0.03079 K_1) \qquad (74)$$

An experimental exhaust hood with a 10 cm diameter orifice was constructed and located with an acetone vapor generator and an organic vapor analyzer (OVA) as shown in figure 12.

A straight blade fan with a 15 cm diameter inlet and powered by a 1/2 hp motor was used to provide exhaust ventilation. The fan was placed inside a fume hood to prevent the re-entrainment of vapors from the exhaust air. A 15 to 13 cm reducer was

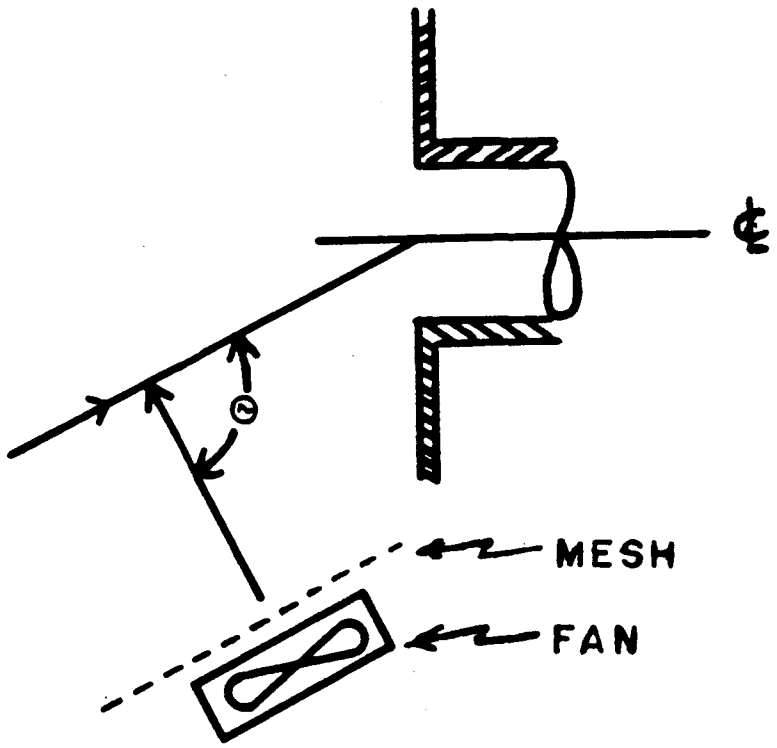

Figure 11. Relationship between jet induced by the exhaust hood and jet used to create the superimposed turbulence.

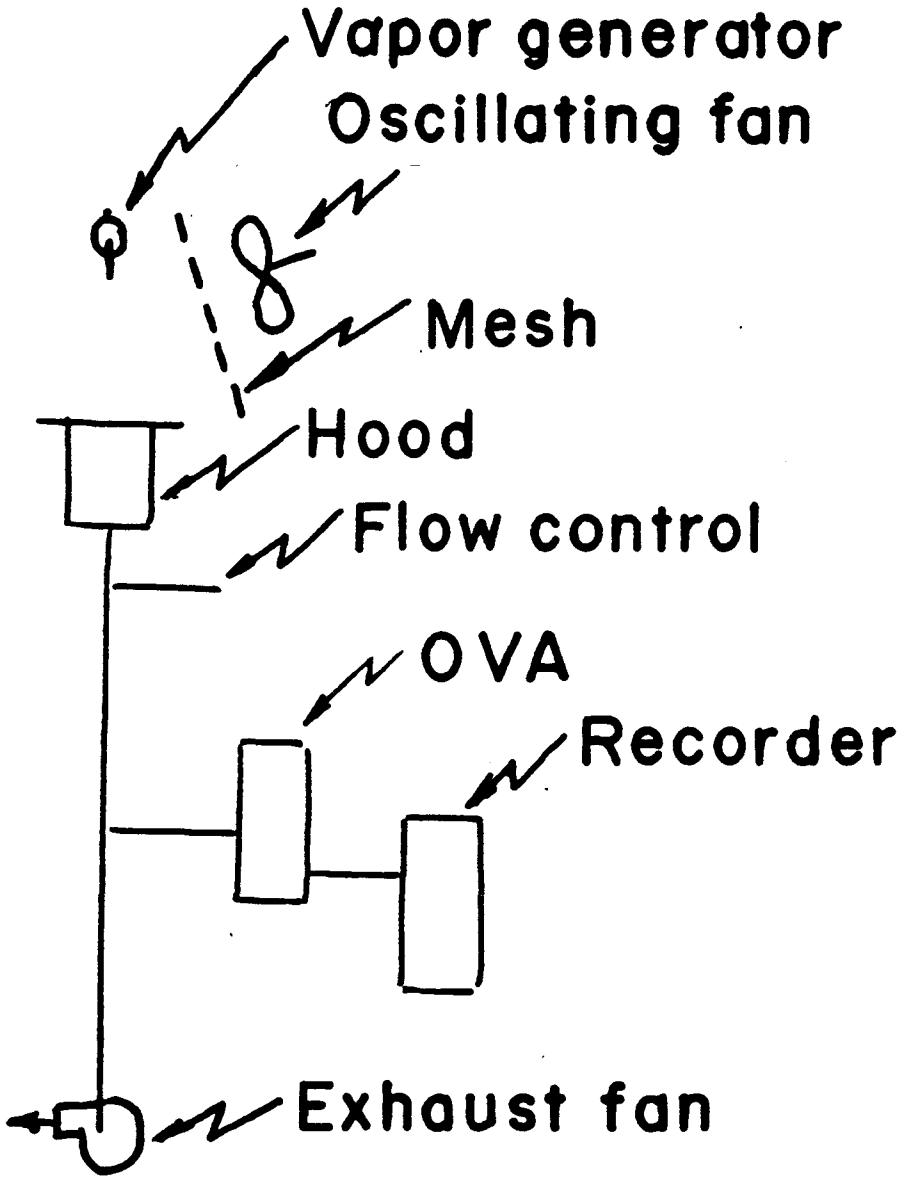

Figure 12. Schematic diagram of the experimental system.

attached to the fan inlet and a 13 cm diameter blast gate was attached to the fan to control the volume of air entering the system. A 13 to 10 cm reducer was attached to the blast gate and 10 cm diameter flexible duct was run to a metal sleeve and elbow. A straight section of metal duct opened into a 30 cm square plenum to which was attached the face piece with a 10 cm diameter circular orifice at its center. In the face piece of the orifice and on the floor below grids were drawn to facilitate positioning of the acetone vapor generating apparatus precisely.

An inclined manometer was placed with the high pressure tap in the straight section of duct downstream from the plenum and the low pressure tap downstream from the elbow. This allowed monitoring of the static pressure drop across the elbow and ensured that constant operating conditions were maintained throughout the experiment.

Acetone vapor was chosen for use in this experiment for several reasons. First, it has a very low toxicity at the concentrations encountered. The experimental runs often lasted three hours or more so that a malfunction somewhere in the system could have created a potentially hazardous situation with a more toxic substance. Second, the distinct odor of acetone would indicate a leak in the system. Third, the OVA responded well to low concentrations of vapor (typical reference concentrations were two ppm) so that small amounts of acetone were consumed during the experimental runs.

The vapor generation apparatus consisted of a pump that

delivered 0.37 ml of air per stroke, a solvent bubbler, a disposable pipette with the tip cut back to provide a larger opening, a heating tape to heat the reservoir of acetone, a variable transformer to control the temperature of the heating tape, and facial tissue for insulating the exposed glass surfaces. It was found that a more consistent reference vapor concentration was maintained using uniformly heated acetone. Since acetone boils at approximately 56 degrees centigrade the generator temperature was maintained 5 degrees below this temperature. The supply air pump outlet was connected to the solvent bubbler using tygon tubing attached to a male coupler which was clamped to the female coupler on the solvent bubbler. The outlet tip was attached to a female coupler using tygon tubing and this was then clamped to the vapor outlet of the bubbler to complete the apparatus.

In operation, the bubbler was filled with acetone to a level at or near the top of the heating tape. The acetone was then heated to 50 degrees centigrade in a fume hood. When the experiment was ready to be run the vapor generator was removed from the fume hood, connected to the pump and positioned for data collection. During the experiment, the acetone was kept at 50 degrees centigrade.

An organic vapor analyzer manufactured by The Foxboro Company was used to measure the acetone vapor concentration in the exhaust air. The air was sampled from the straight duct section immediately downstream from the plenum (figure 12). The

sample was drawn through a teflon tube and into the OVA by the instrument's sampling pump. A strip chart data recorder was used to collect data and provide a record of the experimental runs. The chart paper advanced at a rate of about 2.5 cm/min.

During the experiments the OVA was started and allowed to warm up for a period of 1.5 to 2 hours. The instrument was zeroed to three ppm so that the points recorded by the chart recorder were as discrete as possible, thus facilitating analysis. At the end of each run the instrument was re-zeroed to three ppm to provide a reference for the approximate end of the warm-up period for the next run.

The sampling tube for the OVA was placed in the straight section of duct downstream from the plenum. It was made by bending a piece of 1/8 inch I.D. steel tubing to a 90 degree angle and attaching tubing fittings to one end. The bend was made using a tubing bender so that a smooth curvature of the tubing was obtained. The inlet end of the sample tube was inserted through a hole in the duct and aligned so that the inlet was in the center of the duct and normal to the airflow in the duct. The sample tube was then cemented in place using epoxy putty and as an extra precaution the tubing fittings were clamped in place using a ring stand and a buret clamp. This precaution was found to be unnecessary as the sample tube was accidentally caught and pulled on more than one occasion with no change in the position of the sample inlet.

The superimposed turbulent stream was generated using a

variable speed, three - blade oscillating fan. A variable transformer was used to control the speed of the fan. The variable transformer was powered through a constant voltage transformer to minimize the effects of varying line voltage in the laboratory. In order to provide constant oscillation the oscillator motor in the fan was rewired independently and connected to a separate 120 volt line. A consistent and smooth oscillatory motion was provided by the addition of a centering tension spring. The action of the spring eliminated the end delays frequently found in oscillating fans. By this arrangement a nearly sinusoidal lateral motion was obtained.

A barrier formed by a single thickness of tautly stretched gauze, suspended from the ceiling to the floor, was placed between the fan and the hood. This was used to generate isotropic turbulence.

The rotational speed of the oscillating fan was determined using a stroboscope. The stroboscope was turned on and allowed to warm up and was then calibrated by means of an internal vibrating reed. The stroboscope was calibrated each time it was used and the calibration was checked periodically during operation.

Initially, the speed of the turbulence fan was set using the scale on the variable transformer and the associated rotational speed was determined using the stroboscope. This did not give satisfactory results because there was a significant variation in the fan speed due to slight changes in voltage. Consequently,

the procedure was changed to monitor fan speed during each run and keep it constant.

The coordinate system used to define the location of the experimental points was defined as follows: the geometric center of the orifice was chosen as the origin and was assigned coordinates (0,0,0). Experimental points were assigned values of (0, lateral translation, horizontal translation). As an example the point (0,4,8) was a point located in the horizontal plane of the center of the orifice four inches to the right of the center of the orifice and eight inches back from the plane of the flange. All experimental points were located in the same plane as the center of the orifice and were in a straight line with respect to the center of the orifice. To facilitate positioning of the vapor generator outlet a grid was drawn in one inch squares on graph paper and taped to the platform on which the experiment was located. The grid was positioned so that it was at right angles to the plane of the flange. Once the experimental points were chosen their position was marked on the positioning grid as was the location of the base of the vapor generating apparatus when the tip was positioned at the experimental points. This made positioning of the generator a matter of locating the base at the appropriate place and then adjusting the tip to the exact position. The tip was positioned using a ruler and a right triangle. A vertical line was drawn on the ruler and the height of the center of the orifice was marked. This line was positioned at the point of interest and the

triangle was used to position it vertically. The tip of the vapor generator was then brought up to the mark and the ruler and triangle were removed. This system allowed quick positioning of the tip and hence a maximum amount of time for the system to equilibrate before data collection was begun.

Capture efficiency of the hood was determined by measuring the acetone vapor concentration at a fixed point in the duct. The comparative basis of the efficiency determination was the measurement of acetone concentration with the point of generation just inside the orifice and a similar measurement with the point of generation at the experimental point. The ratio of these measured concentrations of acetone vapor was taken to be the capture efficiency. Every effort was made to ensure that between the reference and experimental measurements the generation parameters of the contaminant were constant. First, the capture efficiency of the hood was determined under quiescent conditions at various points in the field in front of the hood and a map of efficiency isopleths was made. Points were then chosen to examine under turbulent conditions to correspond to points which had 100 percent efficiency under quiescent conditions. A turbulent stream was created with a small oscillating fan separated from the hood flow field by a gauze screen. The screen in front of the fan was necessary to generate isotropic turbulence at the wake of the gauze strands. The capture efficiency was determined as under quiescent conditions. After the capture efficiency was determined for several different

turbulence levels the speed of the turbulent air and the speed of the air entering the exhaust hood was determined using a TSI IFA 100 hot film anemometer.

In the process of the preliminary set up and running of the experiment it was found that if the reference point was chosen as a point approximately one centimeter to the left of the right edge of the orifice in the same plane as the center of the orifice, a much more consistent reading was obtained from the OVA. A comparison of data taken at the point (0,0,0), corresponding to the center of the orifice, and data taken at the point (0,2,0) indicated a much more consistent reading at (0,2,0). Therefore, it was decided to use (0,2,0) as the reference. Although a formal comparison of the data obtained from the two points was not performed, it was assumed, on the basis of the positioning of the tip of the vapor generator relative to the orifice, that all of the vapor generated at the point (0,2,0) was captured by the hood. Comparison of the data collected at the reference point under turbulent and quiescent conditions showed no quantitative differences although there was slightly greater variation in the data collected under turbulent conditions.

The following procedure was followed each time the experiment was run in order to minimize the effects that varying the operational routine might have on the results. This procedure was found to be satisfactory in that the results of experiments repeated on different days were found to be very

consistent.

The first step was to start the OVA per the instructions supplied with the instrument. While the OVA was warming up, the vapor generator was filled with acetone to the level of the top of the heating tape. The top was placed on the generator and the insulating tissue was adjusted so that all of the exposed glass surfaces were covered. The apparatus was always kept in a fume hood except when data was being collected. The heating tape was supplied with 25 volts ac current. This was found to heat the acetone to 50 degrees C.

During the superimposed stream experiments, the secondary fan and the stroboscope used to set the rotational speed of the fan were also started and allowed to warm up. A warm - up period of at least 30 minutes was allowed before the stroboscope and the fan were calibrated.

Once all of the instruments and equipment were satisfactorily warmed up and ready, the exhaust fan was started and the static pressure reading on the inclined manometer was recorded. The system was allowed to operate for a brief period while the face velocity of the exhaust hood was checked with an anemometer. After the face velocity was checked, the strip chart recorder was started and adjusted to 3 ppm.

With the system satisfactorily prepared and operating, the vapor generator was brought from the fume hood and connected to a 30 volt ac source and the pump used to supply air to the apparatus. The tip of the apparatus was not immediately

positioned at the reference point due to the initial surge of vapor which occurred immediately after the pump was started. The vapor generator was allowed to equilibrate for approximately one minute before it was positioned at the reference point. After positioning the tip of the vapor generator at the reference point the system was allowed to equilibrate until such time as the line on the strip chart was level and fluctuating minimally. This usually took approximately five minutes.

Data was collected starting with the reference point followed by three experimental points, then the reference point, then three more experimental points, etc. At the end of a run the reference point was always measured last and the vapor generator was disconnected and moved to the fume hood. If there were to be more experiments run, the vapor generator was kept warm while in the fume hood. Each experimental run covered all of the experimental points to be examined. After each run the OVA and strip chart recorder were readjusted as necessary and the data collection procedure was repeated. Three data points were collected for each experimental point and the results were averaged for the final analysis. The first data collection run started at the point closest to the orifice and would recede from the face of the hood. The second run would start at the most distant point and progress to the closest point, with the third run being a repeat of the first run. Data was collected at each point for approximately three minutes (collection was based on the advancement of the chart paper) with a one minute allowance

for positioning and equilibration. The starting and ending points for each data point were recorded and later transferred to the strip.

The data was analyzed by first tracing a line over the marks on the chart paper. Each experimental point was then demarcated and labeled. The actual analysis was made by examining the tracing and determining the average value of the vapor concentration for that point. To determine the value for the capture efficiency, the reference values bracketing each set of three experimental points was averaged. The capture efficiency was then determined by dividing each experimental value by the average of the reference values bracketing the group in which it lay.

A total of 12 experimental points were examined. They ranged from 0 to 74 cm in a straight line back and in the same horizontal plane as the center of the orifice. Five different rotational speeds were used for the "turbulence fan" : 1115, 1110, 710, 433, and 340 rpm. The exhaust system was set up and operated with the blast gate approximately half open. The blast gate was marked and locked in place for the duration of the experiment and no attempts were made to adjust the flow rate of the exhaust system. This resulted in a face velocity of 24.73 m/sec as measured with the hot film anemometer. The operational static pressure drop across the elbow was found to be approximately 0.63 inches of water. The static pressure drop oscillated slightly during the runs but the variation was less

that +/- .1 inches of water.

Results and Discussion

The results of the measurements of capture efficiency with superimposed stream are shown in Table 5. The graphical representation of the data (figure 13) shows a marked drop in capture efficiency at all of the experimental points, even at the lowest superimposed stream speed. The leveling off is probably due to the recapture of the vapor that was initially dispersed from the experimental point. This leveling off would probably tend to lower efficiency at lower exhaust rates or higher turbulence levels. A similar tailing off of efficiency was seen by Flynn and Ellenbecker (1986). Further investigation of this region is of little practical concern since the efficiency of the hood is less than 50% and it is unlikely that any exhaust system would be intentionally designed and operated in this region.

In a set of experiments, the superimposed stream was fixed orthogonally to the hood stream. The efficiency measurements at different superimposed air speeds did not materially differ from the oscillating stream experiments (figure 14). The fan speeds were chosen to approximate the root mean square cross draft air speeds of the experimental cross draft speeds of 2.2 and 1.2 m/sec. The data was collected at point F and the cross draft air speeds of 0.6 and 1.08 m/sec gave average values of 0.65 and 0.64 for the capture efficiency. This suggests that under the experimental conditions studied, the value of K_1 is small, thus

Table 5

Results of the capture efficiency measurements

	Average capture efficiency measured					
	Calm air	1115 rpm	1110 rpm	710 rpm	433 rpm	340 rpm
air speed m/sec	0	2.15	2.17	1.18	0.49	0.43
Point						
A	-	.71	.73	.73	.76	.85
B	1.18	.77	.78	.77	.81	.88
C	1.12	.77	.78	.79	.82	.87
D	1.11	.74	.74	.74	.78	.84
E	1.11	.66	.68	.75	.75	.79
F	1.10	.57	.55	.69	.75	.78
G	1.08	.50	.46	.61	.75	.78
H	1.10	.43	.44	.51	.74	.77
I	1.01	.43	.42	.47	.71	.76
J	1.03	.38	.39	.46	.70	-
K	1.01	.34	.37	.42	.69	-
L	.92	.32	.37	.40	.66	-

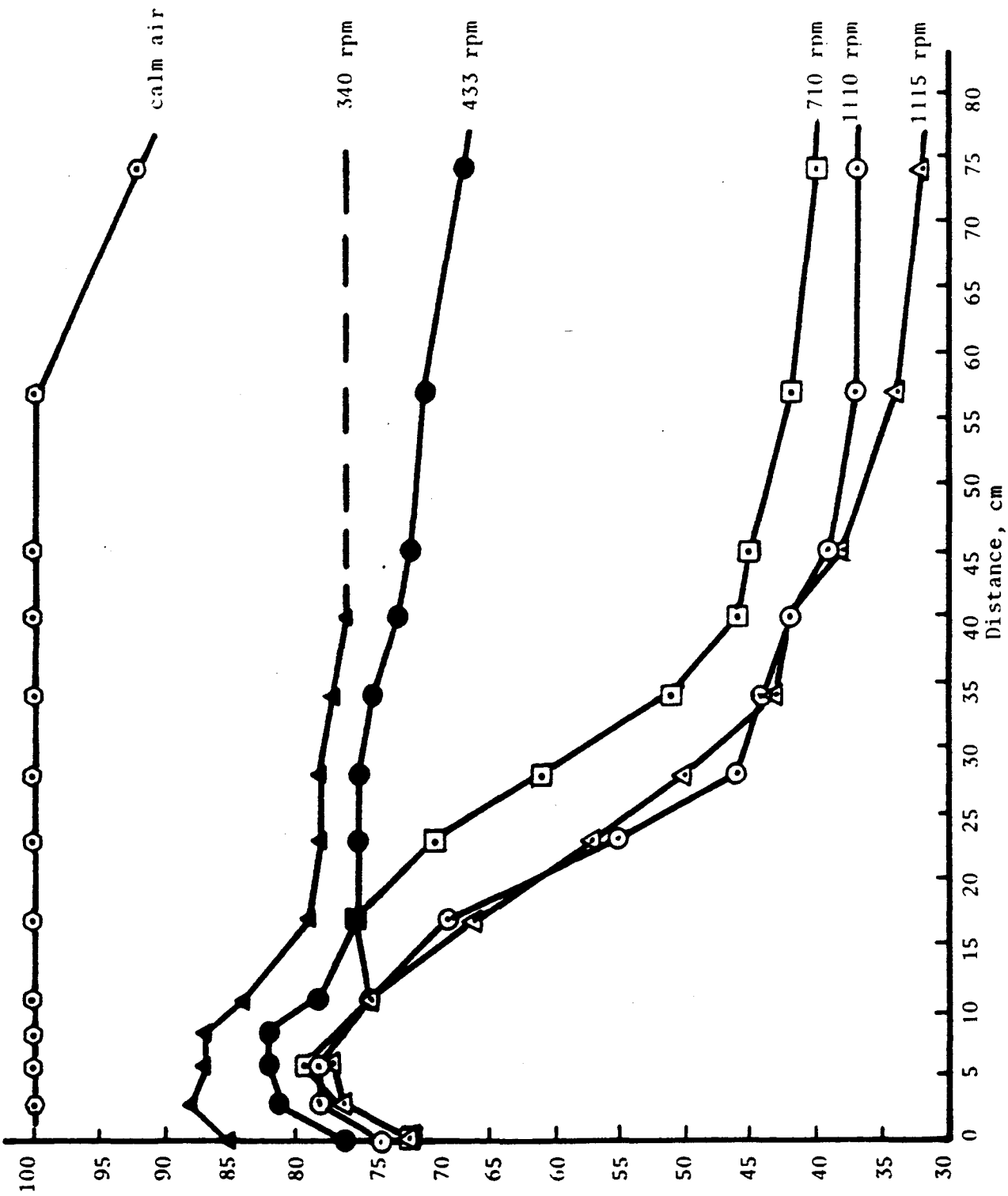

Figure 13. Capture efficiency as a function of distance from the center of the orifice.

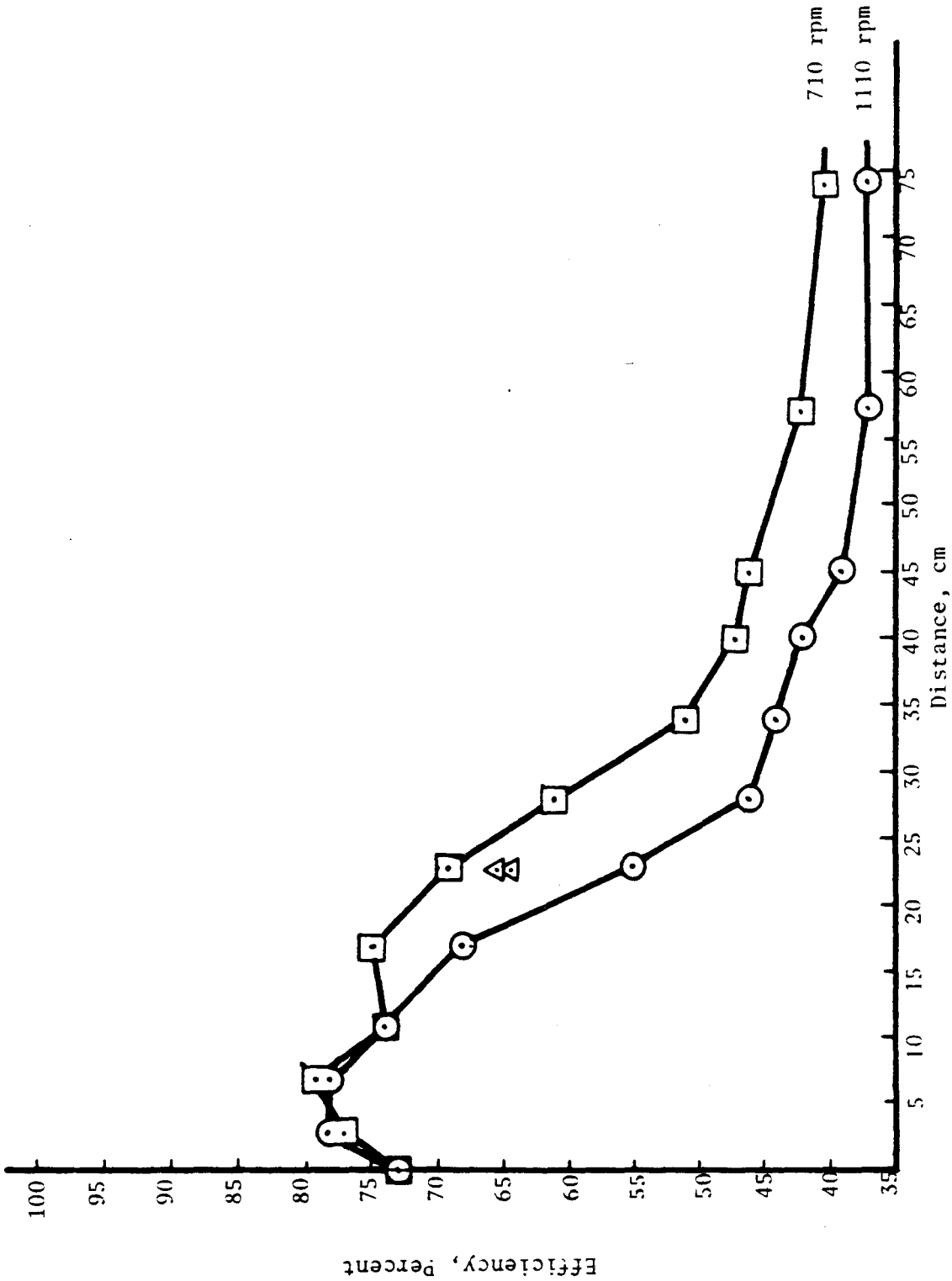

Figure 14. Comparison of efficiency reduction by orthogonal cross draft with the corresponding oscillating cross drafts

the change in efficiency is dominated by the effects of turbulence. Consequently, the experimental results provide a convenient avenue to develope a semi-empirical relationship using equations 71 and 73.

Figure 15 is a plot of -log(efficiency) versus the ratio of superimposed stream air speed to hood generated air speed for the data from seven of the points examined. These results suggest that K is approximately equal to K_s thus n = 1/6. This in turn suggests a value of approximately .35 to the constant K_0 . The semi-empirical correlation for the system studied may be expressed as:

$$E_s = E_c \exp \left[-.35 \left[1 + K_1 \cos(\theta/2) \right] \left[\frac{U_s}{U_h} \right]^{1/6} \right] \quad (74)$$

This equation is consistent, as hood generated air speed goes to zero, the capture efficiency will go to zero and as superimposed air speed goes to infinity, the capture efficiency will go to zero and the hood efficiency will be simply the amount induced into a general ventilation system. The implications of these results are important. Simple calculations with equation 74 will show that a relatively small but highly turbulent cross draft about 5 percent of the point speed of the hood generated air motion will lead to about 20 percent loss in the hood efficiency. Such highly turbulent cross drafts are common occurrences in the wakes of blunt bodies moving at relatively small (20-30 000) Reynolds' numbers. This observation will imply that the observed loss of efficiency of hoods due to normal performance of tasks in front of a hood in the work place can be

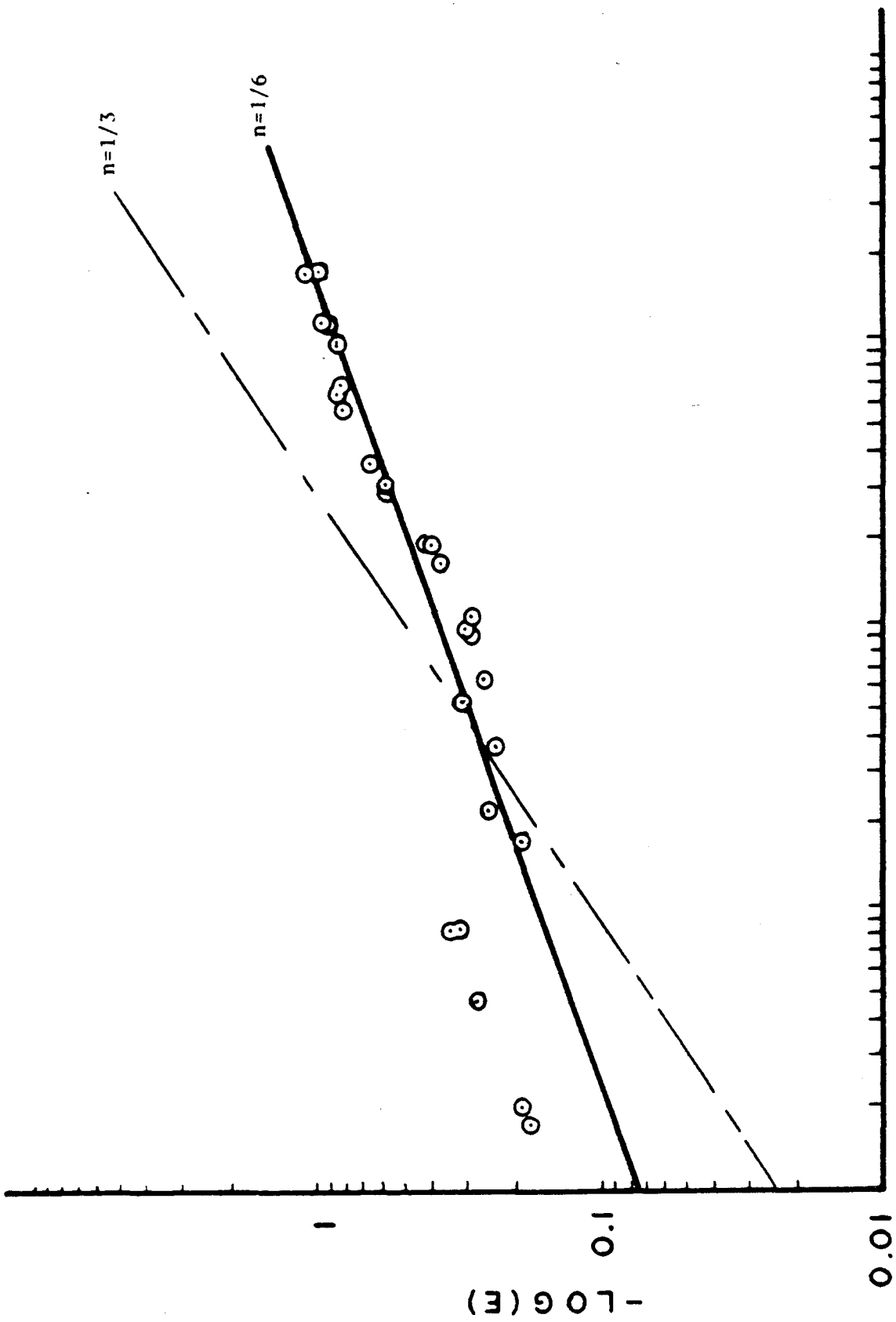

Figure 15. Plot of -log(efficiency) versus ratio of superimposed air speed to hood induced air speeds for seven representative locations.

explained to a large extent through turbulent mixing. It is also interesting to note that the characteristics of the interference are highly dependent upon the ability of the superimposed airstream to mix the contaminant with the general room air. These characteristics imply that the modification of the capture of contaminants is expected to be influenced by the characteristics of the contaminant as well. For example, a contaminant mostly composed of particles larger than a few microns will be less effected than contaminants mostly composed of smaller particles. This will suggest that in the case of small particles a preferential reduction of capture efficiency of an exhaust hood is expected. These results raise important questions in terms of the prediction of the performance of capture hoods.

Conclusions:

These experiment were performed to evaluate the effects of turbulence on the capture efficiency of a free standing exhaust hood. The results show a surprisingly strong influence. It was shown that even low levels of turbulence, weak cross currents can have a dramatic effect on the capture efficiency of an exhaust hood. As it can be seen in figure 13 at the lowest superimposed cross draft air speed of 0.43 m/sec (340 rpm), there was a 15% loss of capture efficiency in the region within two duct diameters distance from the hood opening. This region is normally considered to be fully under the influence of the exhaust system,

yet the measurable drop in capture efficiency is clear. This loss of capture efficiency at low cross draft speeds indicates that the turbulence created at these low speeds can not be ignored in the design and evaluation of the ventilation systems.

The semi-empirical equation developed to express the efficiency of the hood indicates that the presence and motion of a worker in the capture zone of the hood has the potential to significantly reduce the capture efficiency of the hood. Ideally, automation would be the best way to improve capture efficiency. It would remove the worker from exposure and allow the contaminant source to been closed thus allowing the use of smaller ventilation systems. Where automation is not feasible the worker must be considered an integral part of the process and his presence in the capture zone must be included in the design of the exhaust hood.

Current design criteria specify a capture velocity based on qualitative properties of the contaminant material. Velocities are specified on the basis of the nature of the contaminants which are described as vapors, gases, smoke, fumes, very fine light dust, dry dusts and powders, average industrial dust, heavy dusts, heavy or moist dusts. Clearly, these are subjective appraisals of the materials and do not necessarily relate to their behavior as an aerosol nor do they address the nature of the process by which they are generated. It is known that the motion of particles on the order of 0.5 microns in diameter and smaller is governed primarily by diffusion rather than

gravitational settling. It is also an accepted fact that it is these small particles that are the critical from the standpoint of exposure via inhalation. This work demonstrated that turbulent diffusion caused by a superimposed cross draft has a significant effect on the capture efficiency of an exhaust hood. Thus it is clear that two sources of a single contaminant producing fine (respirable/inhalable) and coarse (inhalable/not respirable) particles will not be controlled to the same degree under identical conditions. Such factors as the placement of the worker relative to the orifice and the configuration of the contaminant source should be considered in addition to the minimum velocity needed to control the contaminant. The behavior of gases and vapors is expected to be identical to that of the air in which they are dispersed in most situations. Naturally, those gases and vapors which are generated under high pressure must be treated differently since the jet of contaminant will create its own turbulence. Another obvious implication of this work is the need to minimize the cross drafts present in any area where local exhaust ventilation is being used. The weaker cross drafts used in this experiment were barely perceptible to the hand yet they had a profound effect on the capture efficiency of the hood. The magnitude of the effects of the cross draft are perhaps best illustrated in figure 16 which are selected from a series of pictures taken using a smoke generator placed at one of the experimental points. The first picture shows the hood operating with no cross draft present. It can be clearly seen

that all of the smoke is moving directly into the hood without much dispersion of the plume. This occurred even though the smoke was leaving the generator at a high speed. The next picture was taken with the fan running at 710 rpm. The picture clearly shows the smoke being dispersed by the fan and in fact the disruption was such that the smoke generator could only be operated for brief periods before the hood face was obscured by the smoke.

It must be emphasized that this work was far from an exhaustive study of the problem. The hood was of the simplest geometry and all possible precautions were taken to minimize any but the desired interfering factors. The quiescent capture efficiency of the hood was characterized in only two dimensions and the experimental points lay in a single straight line back from the orifice. In view of the dramatic effects observed, further and more detailed study with different shape hoods, three dimensional profiles, etc. is not warranted; because the observed effects were produced under what may be considered to be best capture conditions.

Figure 16. Hood operating with no and 1.2 m/sec cross draft

ADDITIONAL RESEARCH FINDINGS:

Certain amount of ancillary calculations, measurements and research as supported by this grant is reported in the literature. These reports are included in appendix 2. In addition to the reported results, the principal investigator has a substantial amount of unanalyzed data as the result of this study. As the analyses of these data is completed and published, NIOSH will be provided with the preliminary and final copies of the ensuing articles.

LITERATURE CITED:

1. Bers, L. and Gelbart, A.; Trans. Amer. Math. Soc., 56:67-93, (1944).

2. Braconnier, R.; Champs de vitesse au voisinage de l'entree des dispositifs d'aspiration localisee, Cahiers de Notes Documentaires, No:124, 265-289, (1986).

3. Comte-Bellot, G.; Hot-wire anemometry, Annual Review of Fluid Mechanics 8:209-231, (1976).

4. Corrsin, S. "The isotropic turbulent mixer: Part II Arbitrary Schmidt Number" A.I.Ch.E. Journal, 10:870-877 (1964).

5. Coulson,J.M. and N.K. Mitra; "The mixing of solid particles" Ind. Chem 26:55-60 (1950).

6. Dallavalle, J.M.; "Studies in the design of local exhaust hoods." Doctoral Dissertation, Harvard University, Boston, MA, (1930).

7. Esmen, N.A., D.A. Weyel & F.P. McGuigan; Aerodynamic Properties of Exhaust Hoods, Amer. Ind. Hyg. Assoc. J., 47:448-454, (1986).

8. Esmen, N.A. and D.A. Weyel; Aerodynamics of multiple orifice hoods, Ventilation 1985, Elsevier H.D. Goodfellow (Edit.) New York, p. 735-743, (1986).

9. Esmen, N.A., D.A. Weyel, A. Pirris and A. G. Ilori; Aerodynamics of Arbitrarily shaped orifice exterior hoods. This work, (1990).

10. Fletcher, B.; Effect of flanges on the velocity in front of exhaust ventilation hoods. Ann. Occup. Hyg., 21:265-269;(1978).

11. Fletcher, B. and A.E. Johnson; Velocity profiles around hoods and slots and the effects of an adjacent plane. Ann. Occup. Hyg., 25:365-372; (1982).

12. Flynn, M.R. and M.J. Ellenbecker; Capture efficiency of flanged circular local exhaust hoods. Ann. Occup. Hyg., 30:497-513; (1982).

13. Flynn M.R. & M.J. Ellenbecker; The potential flow solution for airflow into a flanged circular hood., Amer. Ind. Hyg. Assoc. J., 46:318-322, (1985).

14. Flynn, M.R. and M.J. Ellenbecker; "Capture efficiency of flanged circular local exhaust hoods" Ann. Occup. Hyg. 30:497-513 (1986)

15. Flynn, M.R. & M.J. Ellenbecker; Empirical validation of theoretical velocity fields into flanged circular hoods., Amer. Ind. Hyg. Assoc. J., 48:380-389 (1987)

16. Jorgensen, F.E.; Directional sensitivity of wire and fiber film probes, Disa Information II:31-37, (1971)

17. Lamb, H.; Hydrodynamics Sixth Edition Dover Publications, New York p.73 (1945)

18. Menchoff, D.; Les Conditions de Monogeneite Hermann et Cie, Paris p.329 (1939)

19. Prandtl, L. and O.G. Tietjens; Fundamentals of Hydro- and Aeromechanics , Dover Publications, New York; (1957).

APPENDIX I

Graphical Representation of Experimental Results

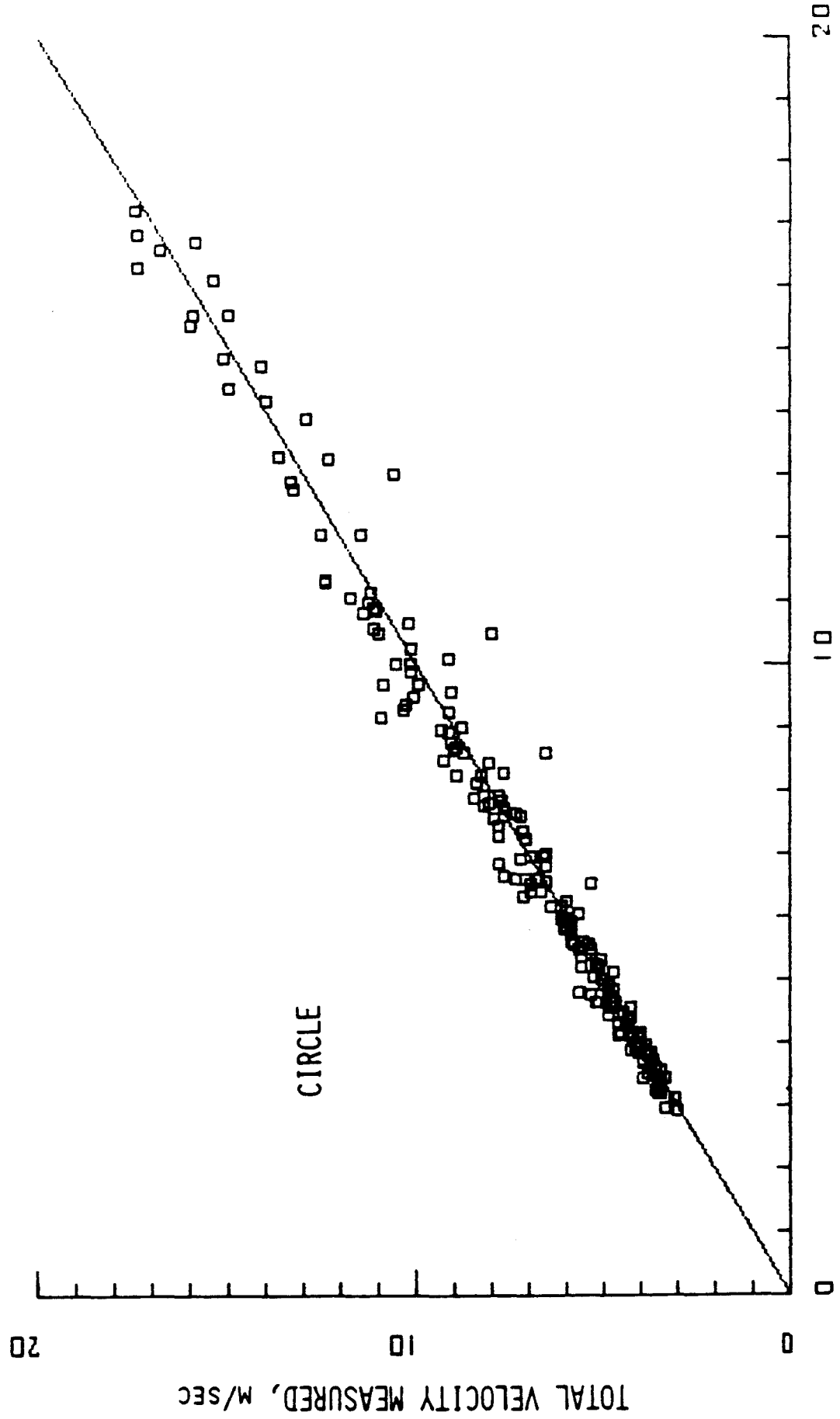

Figure A1. Comparison of calculated and measured total velocity for a circle orifice hood.

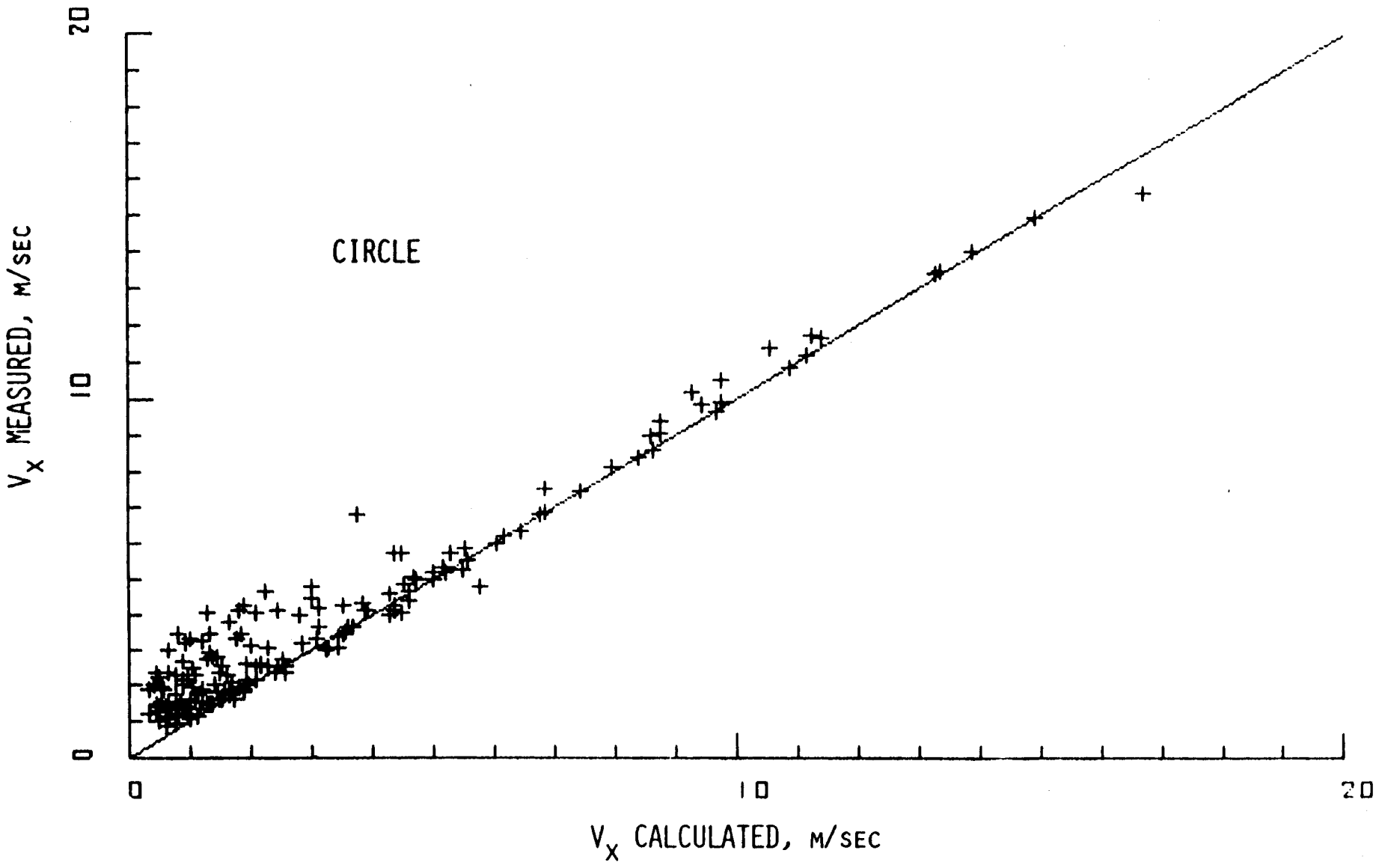

Figure A2. Comparison of calculated and measured x component of velocity for a circle orifice hood.

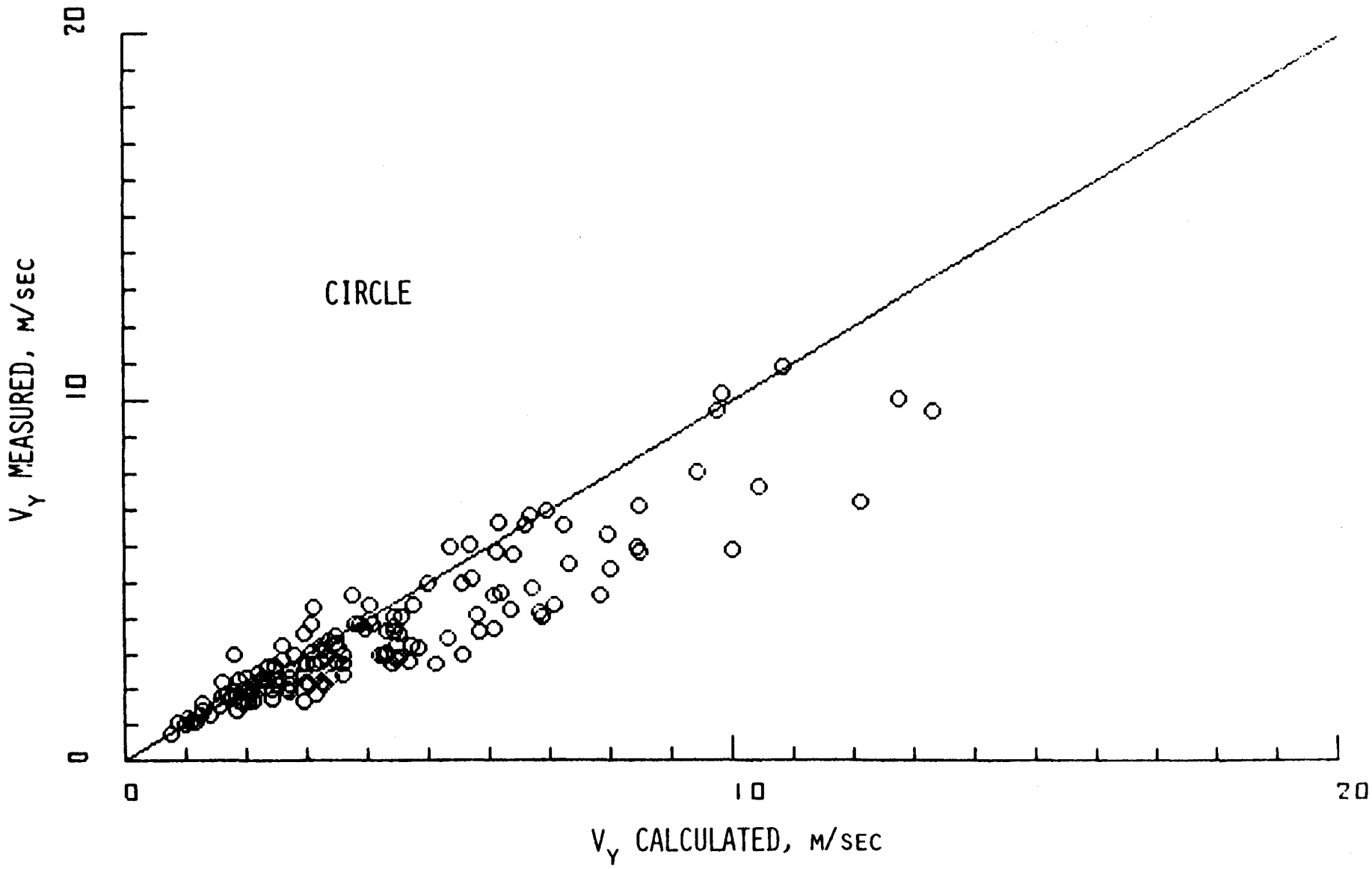

Figure A3. Comparison of calculated and measured y component of velocity for a circle orifice hood.

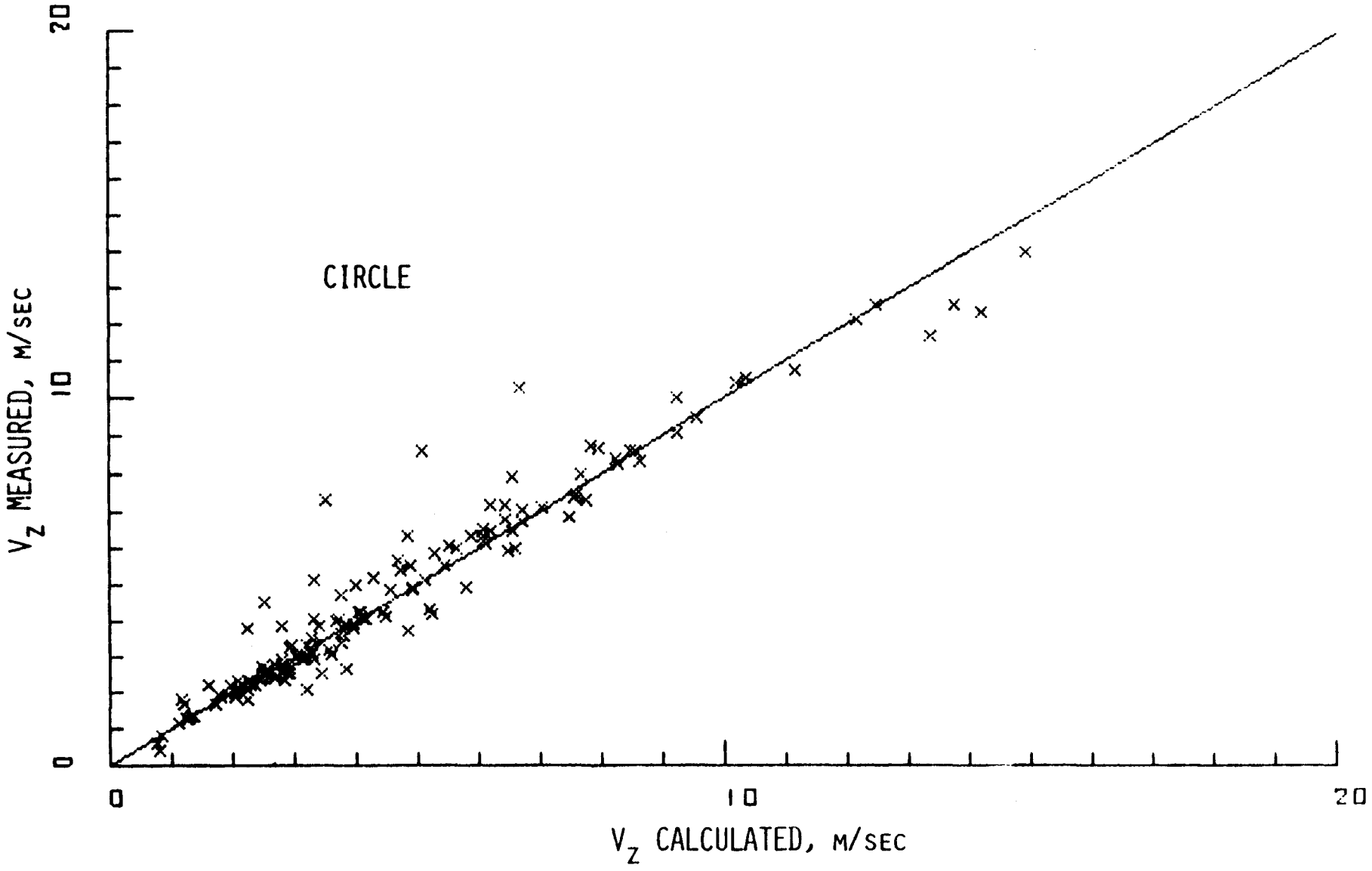

Figure A4. Comparison of calculated and measured z component of velocity for a circle orifice hood.

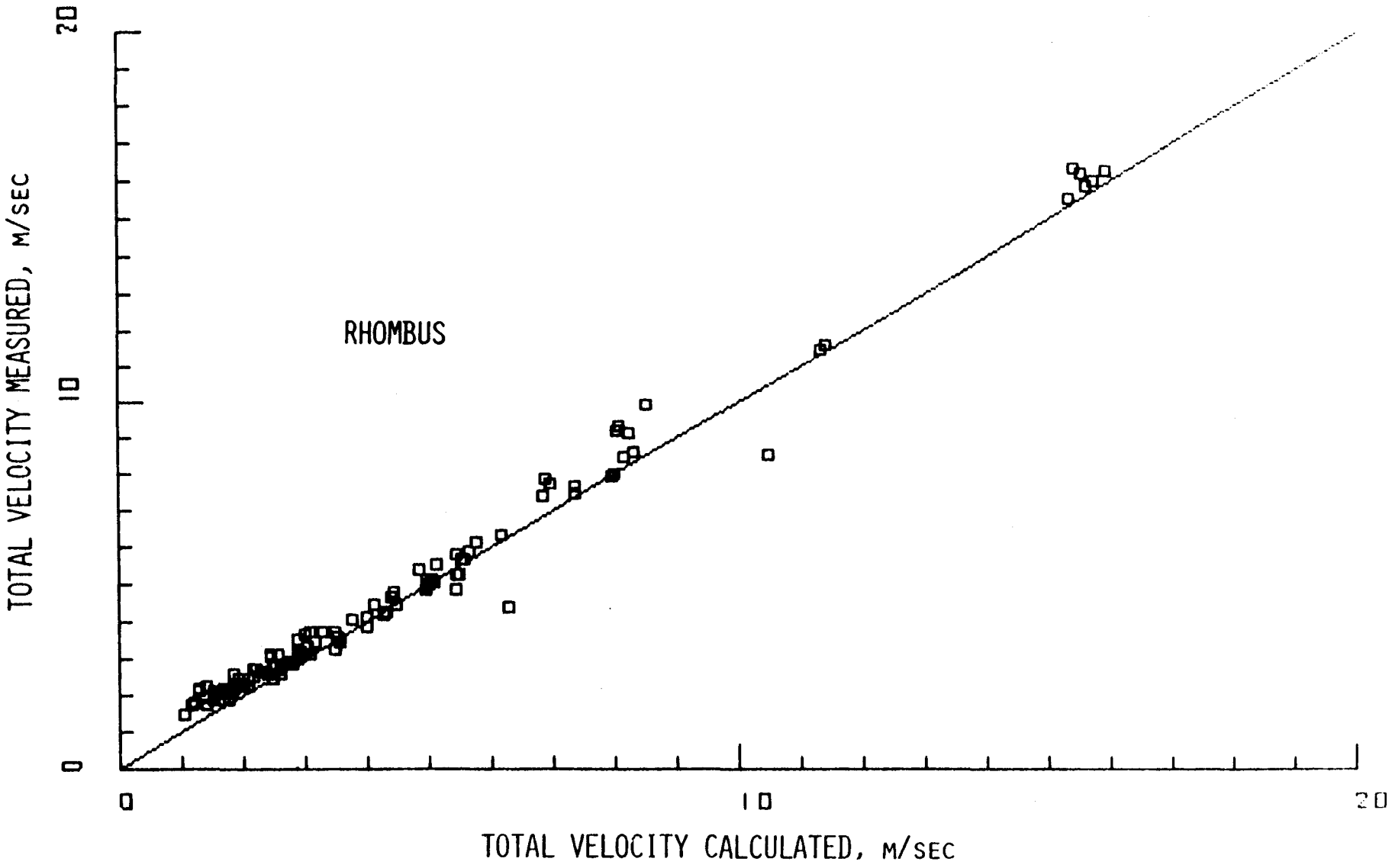

Figure A5. Comparison of calculated and measured total velocity for a rhombus orifice hood.

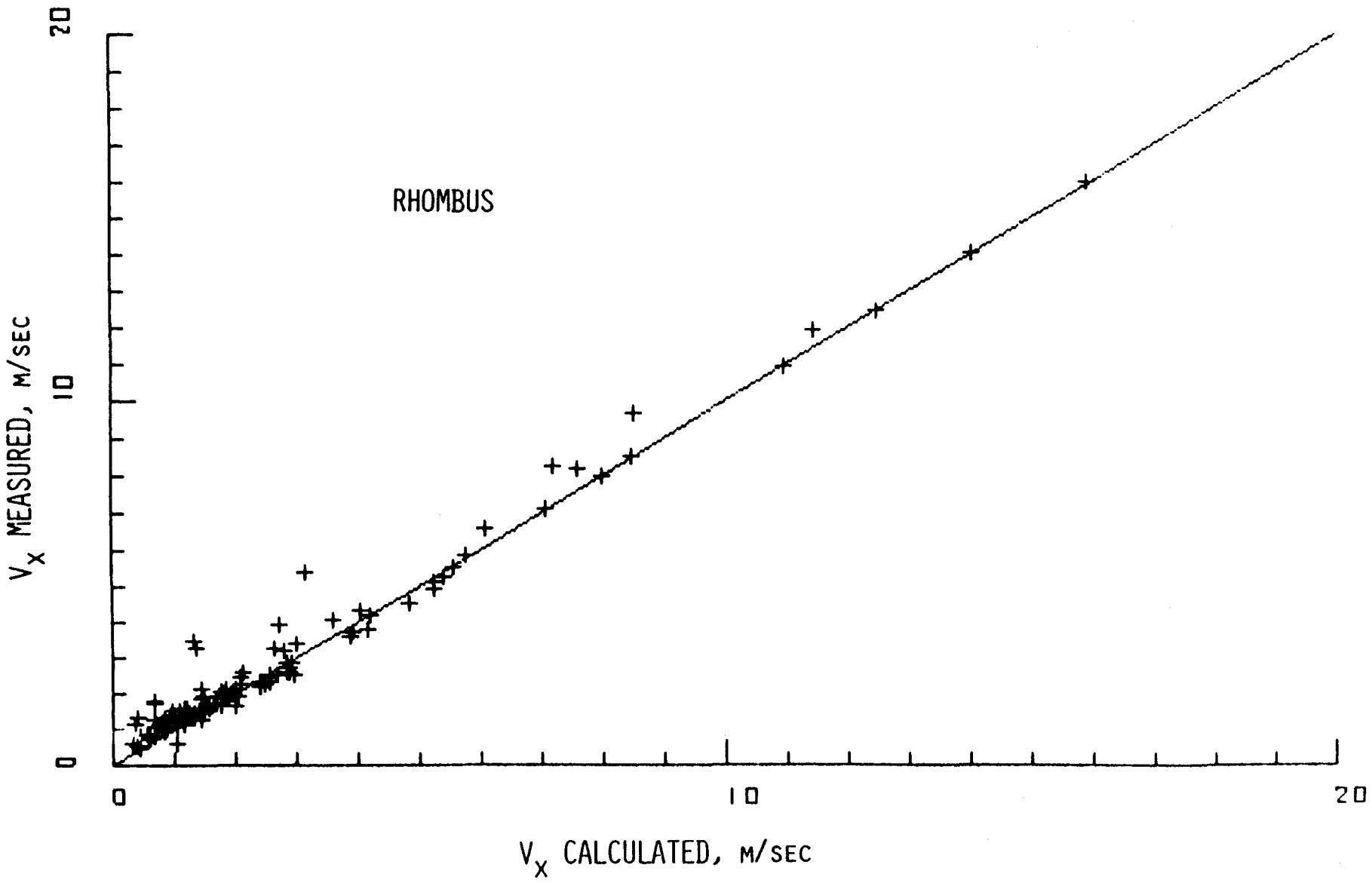

Figure A6. Comparison of calculated and measured x component of velocity for a rhombus orifice hood.

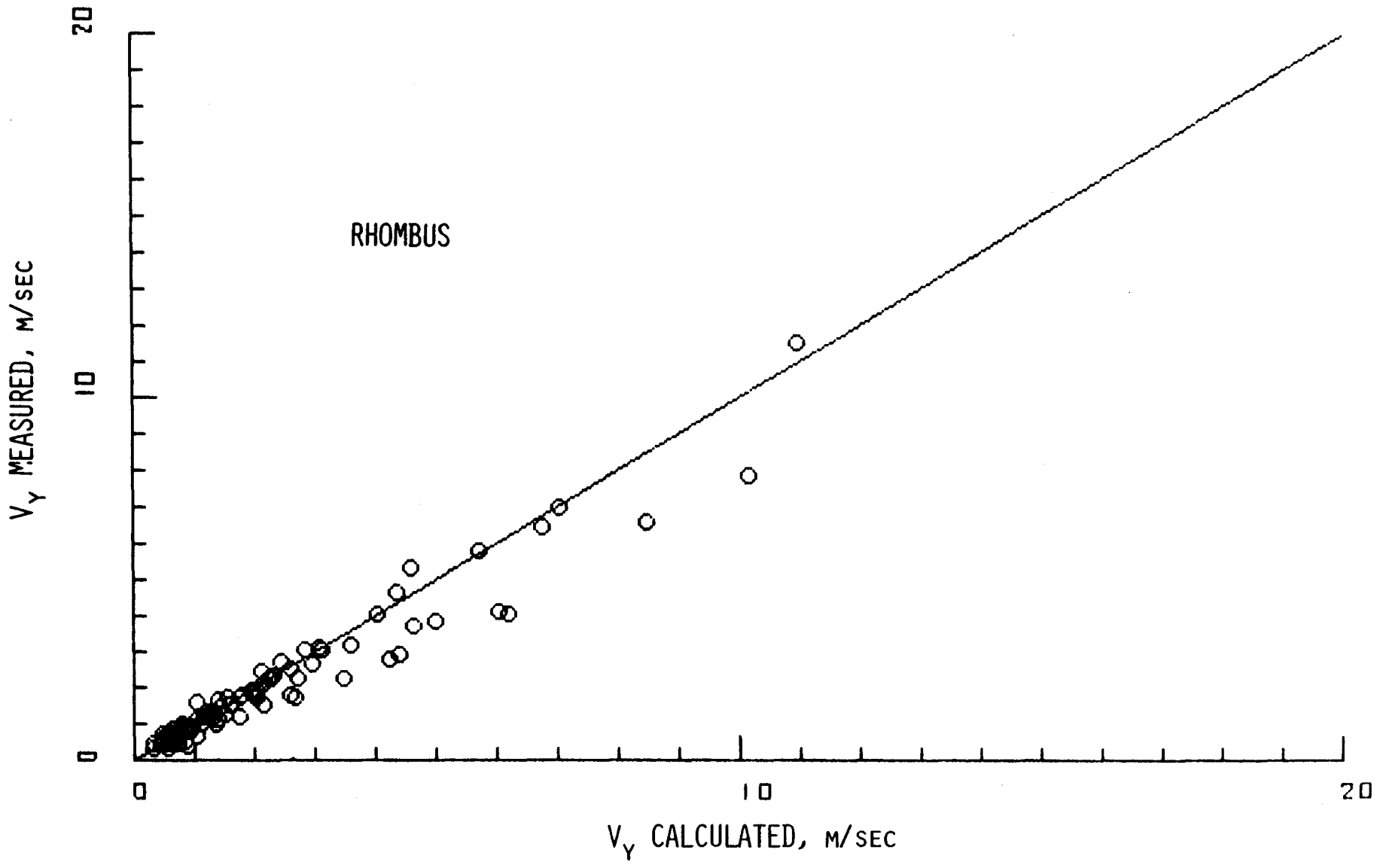

Figure A7. Comparison of calculated and measured y component of velocity for a rhombus orifice hood.

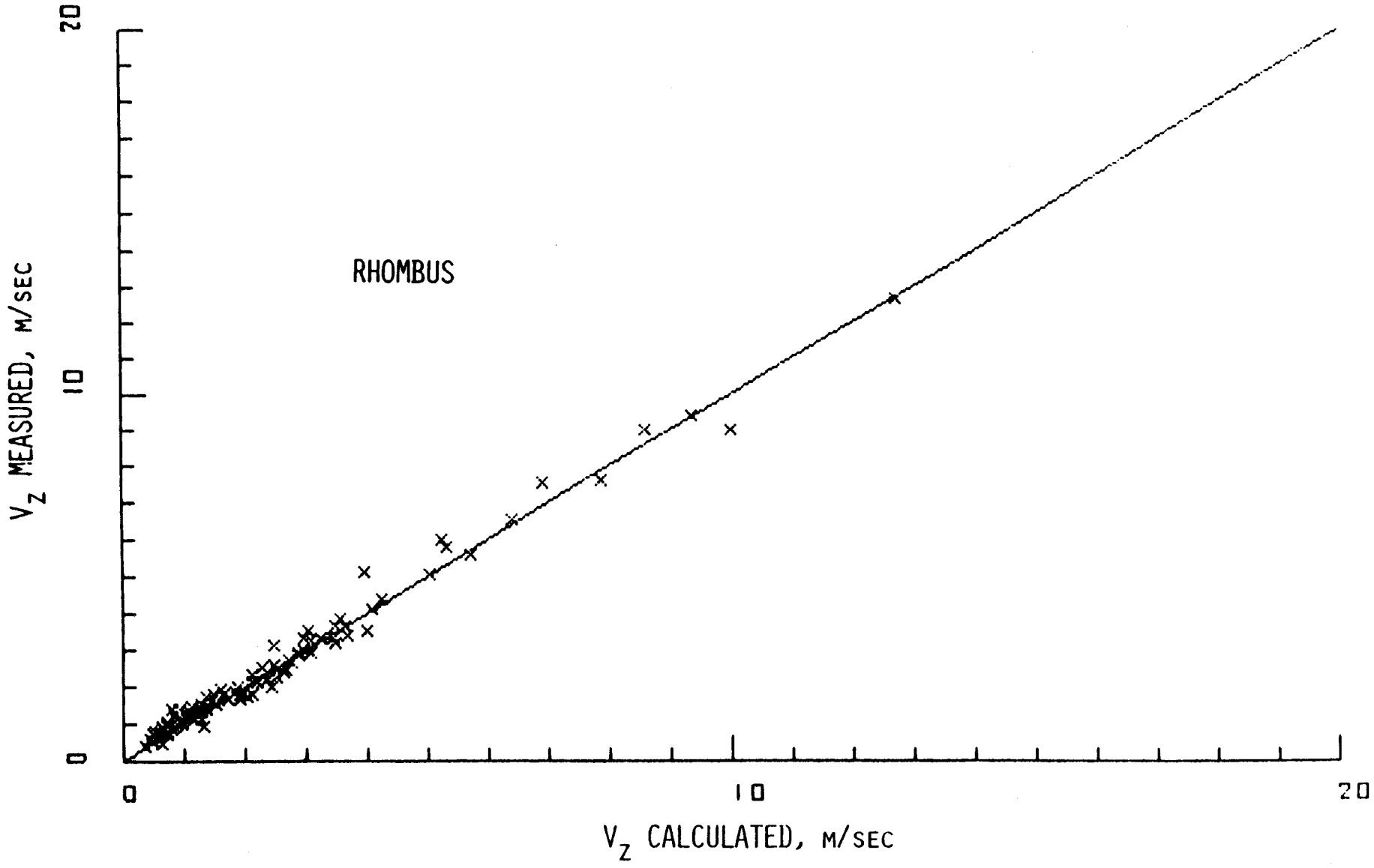

Figure A8. Comparison of calculated and measured z component of velocity for a rhombus orifice hood.

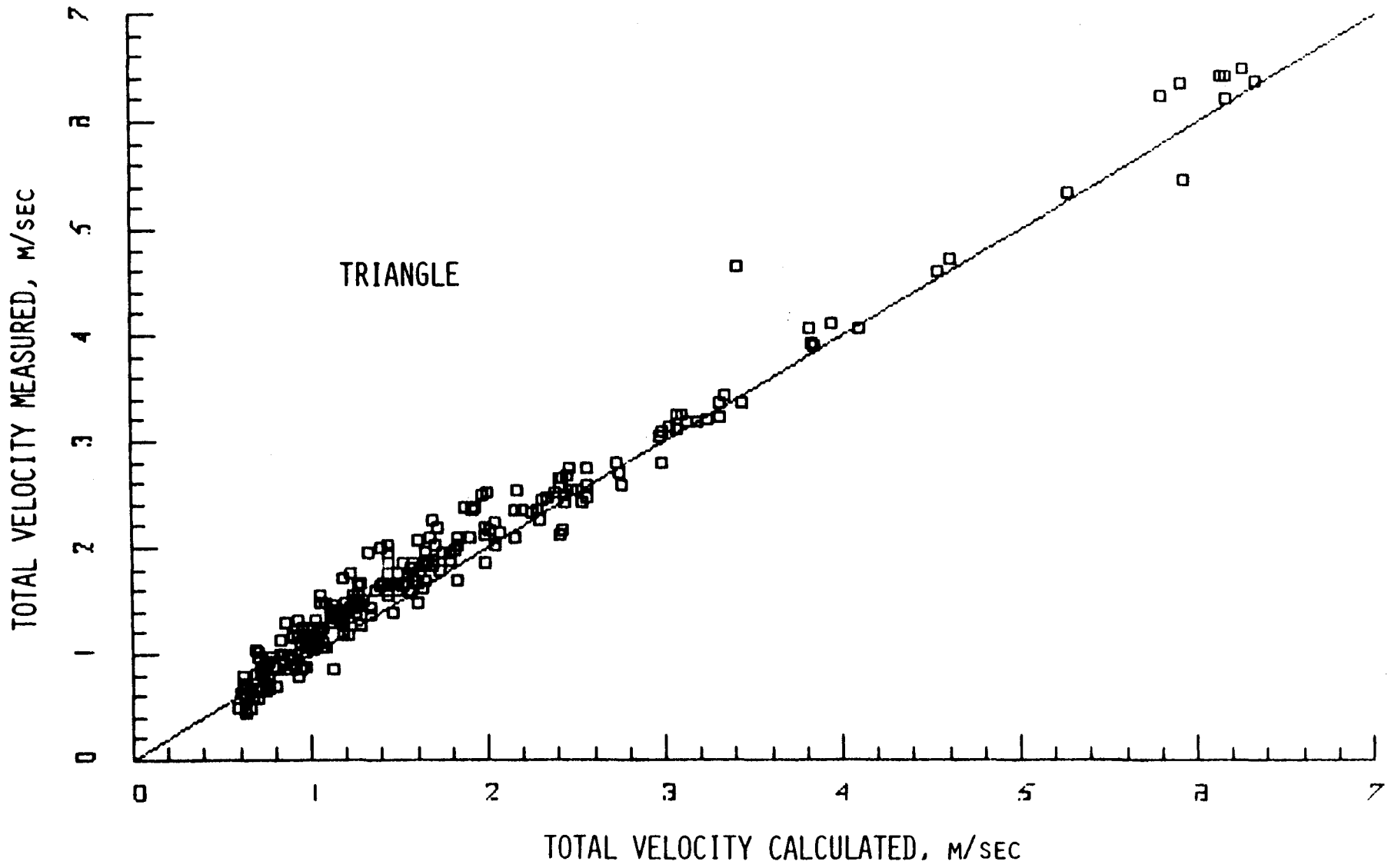

Figure A9. Comparison of calculated and measured total velocity for a triangle orifice hood.

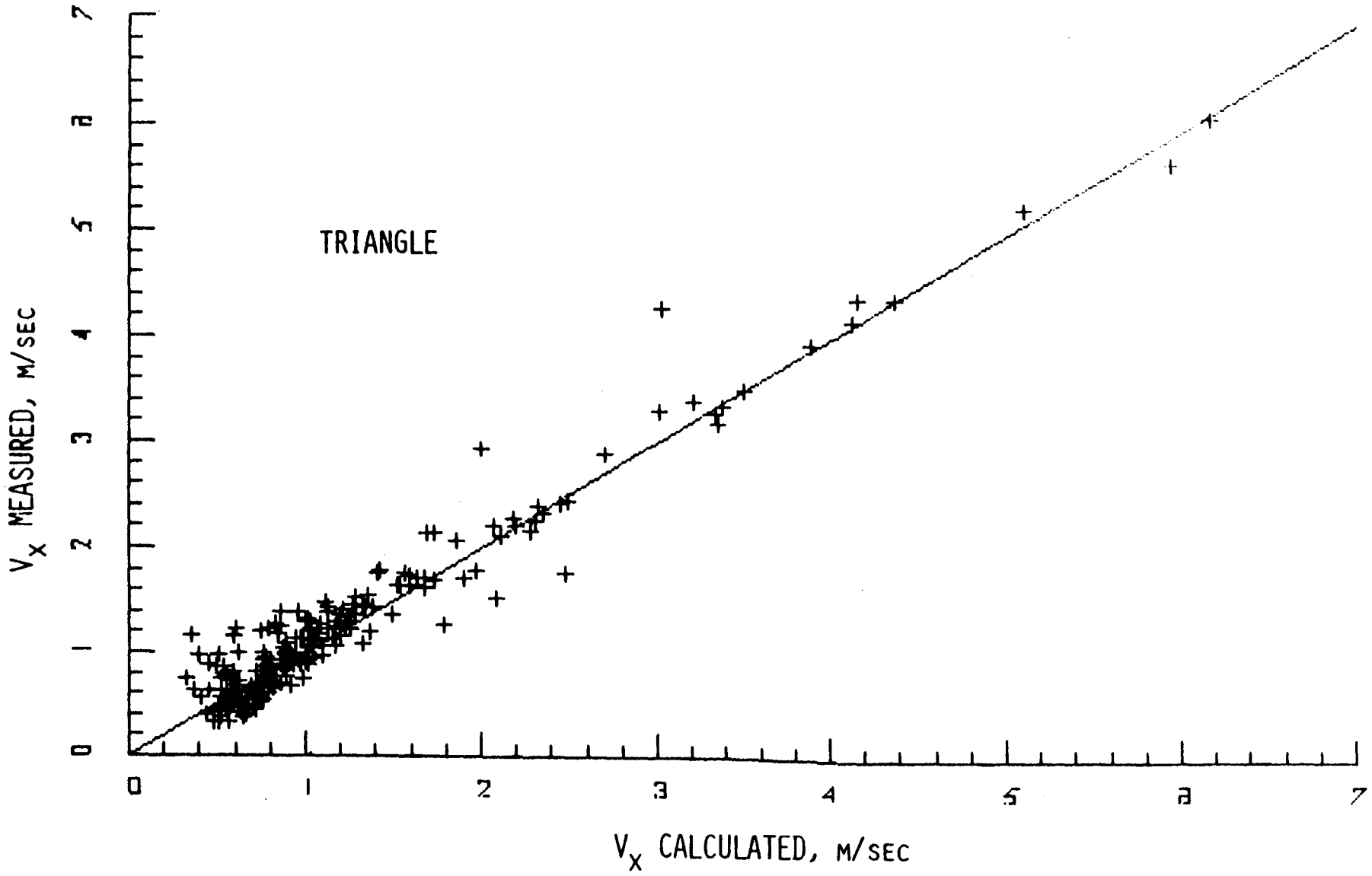

Figure A10. Comparison of calculated and measured x component of velocity for a triangle orifice hood.

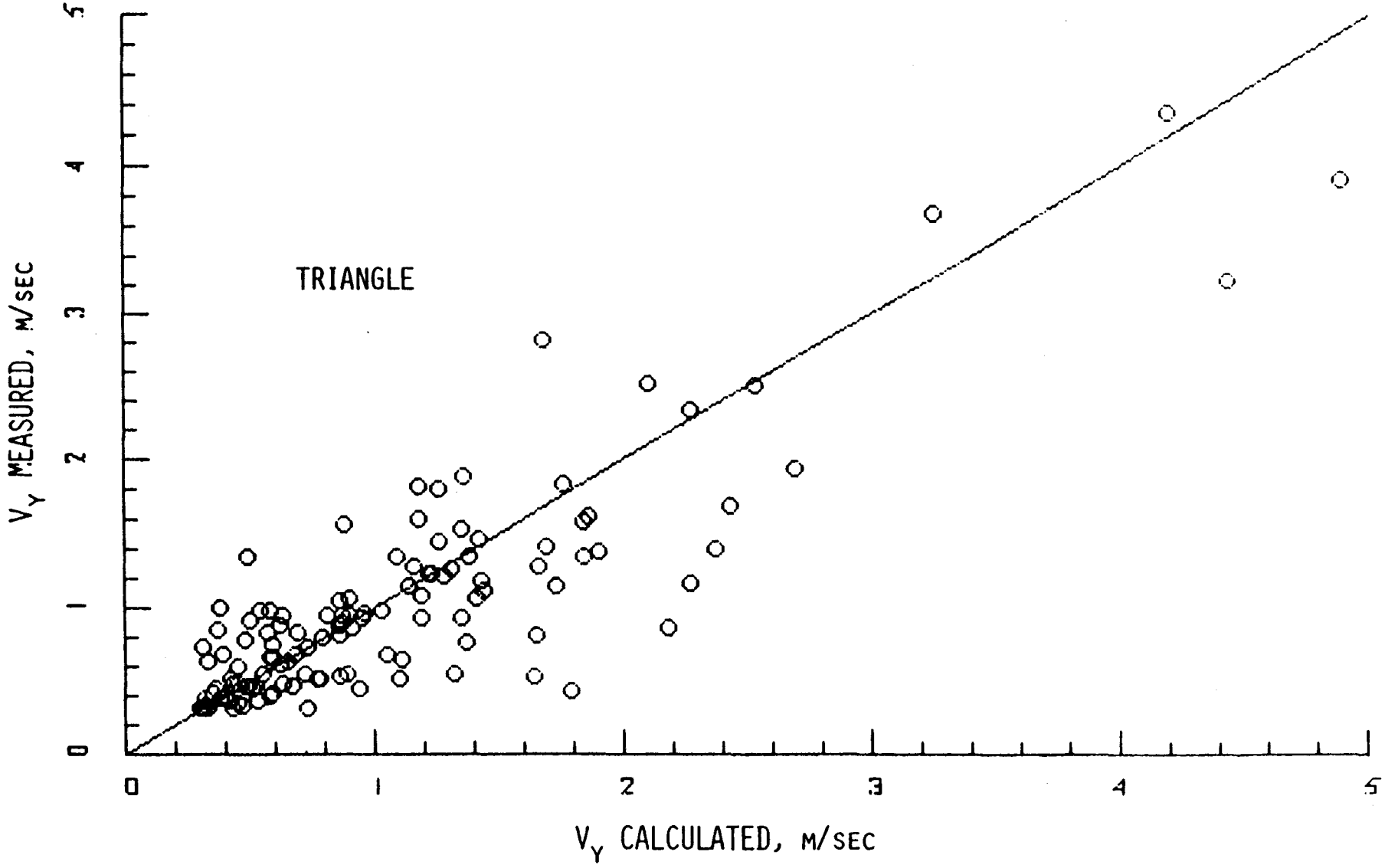

Figure A11. Comparison of calculated and measured y component of velocity for a triangle orifice hood.

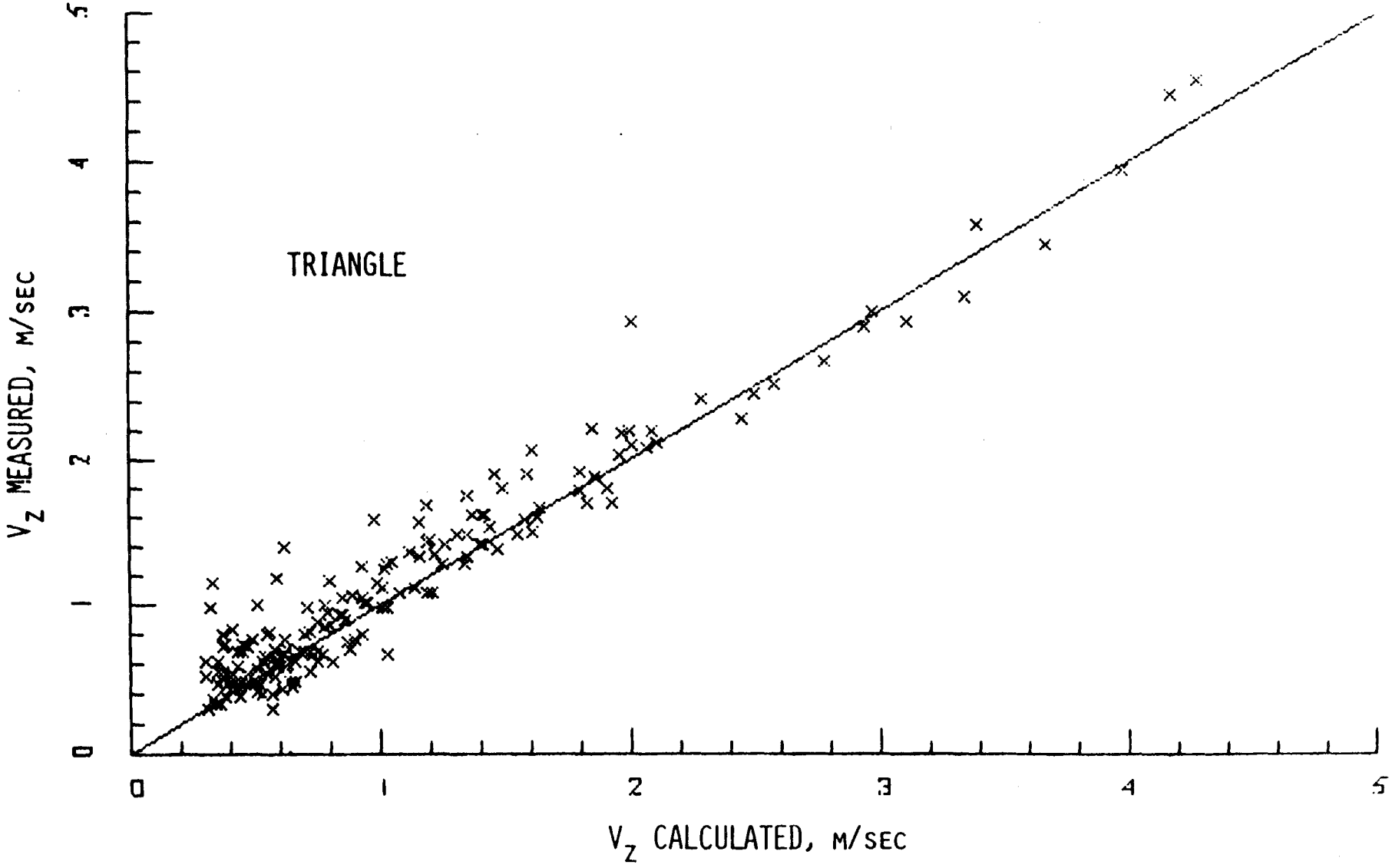

Figure A12. Comparison of calculated and measured z component of velocity for a triangle orifice hood.

APPENDIX II

Published Papers and Symposia Proceedings

Publications

Esmen NA, Weyel DA: Air Flow Generated by Flanged Suction Hoods with Adjacent Planes. Ventilation '88. (ed. JH Vincent), Pergamon Press, London, in press, 1988

Esmen NA, Weyel DA: Optimization of Freely Suspended Exterior Hoods in Industrial Ventilation. Proceedings VIIth International Pneumoconioses Conference, in press, 1988

Esmen NA, Weyel A, Pirris A, Ilori AG: Aerodynamics of Arbitrarily Shaped Orifice Exterior Hoods. Ann Occup Hyg, in press, 1988

Durr DE, Esmen NA, Stanley C, Weyel DA: Pressure Drop in Flexible Ducts. Applied Ind Hyg 2:99-102, 1987

Durr DE, Esmen NA, Stanley C, Weyel DA: Pressure Drop in Elbows. Applied Ind Hyg 2:57-60, 1987

Esmen NA: Numerical Expressions for Ventilation Parameters. Ventilation '85. (ed. HD Goodfellow), 735-743, 1986

Esmen NA, Weyel DA: Aerodynamics of Multiple Orifice Hoods. Ventilation '85. (ed. HE Goodfellow), 735-743, 1986

Unpublished Articles

Final Report, Nurtan A. Esmen, Fundamental of Exhaust Hoods, August 13, 1990

Esmen NA, Weyel DA, Pirris A: Design Parameters for Freely Suspended Exterior Hoods. Amer Ind Hyg Conf, Montreal, Canada, 1987 (Abstract)

Esmen NA, Weyel DA: Aerodynamics of Exterior Hoods with Flanking Planes. Amer Ind Hyg Conf, Montreal, Canada, 1987

Weyel DA, Durr DE, Esmen NA: Multiple Orifice Hoods. Amer Ind Hyg Conf, Dallas, Texas, 1986 (Abstract)

50272-101

REPORT DOCUMENTATION PAGE	1. REPORT NO.	2.	3. PB91-173393
4. Title and Subtitle Fundamental Investigation of Exhaust Hoods			5. Report Date 1990/08/00
			6.
7. Author(s) Esmen, N. A., D. A. Weyel, T. A. Grauel, A. G. Ilori, S. Jossell, and A. Parris			8. Performing Organization Rept. No.
9. Performing Organization Name and Address Department of Industrial Environmental Health Sciences, Graduate School of Public Health, University of Pittsburgh, Pittsburgh, Pennsylvania			10. Project/Task/Work Unit No.
			11. Contract (C) or Grant(G) No. (C) (G) R01-OH-02132
12. Sponsoring Organization Name and Address			13. Type of Report & Period Covered
			14.

15. Supplementary Notes

16. Abstract (Limit: 200 words) This study investigated the theoretical aspects of airflow in front of freely suspended flanged hoods with arbitrarily, but symmetrically shaped hood orifices. Results indicated that an extension of the superimposition of two virtual sinks and potential flow assumption to describe the flow field can be used. The observed effect of turbulence on the capture efficiency of hoods and the magnitude of the reduction of the capture efficiency with what might be considered to be a relatively mild turbulent cross draft. Experimental data indicated that a turbulent cross draft in the order of 5 to 10% of the hood induced air speed in the mean velocity magnitude can reduced the overall capture efficiency of a hood by 15%. Using a conformal mapping technique, the theoretical investigations were also extended to include hoods with adjacent planes of arbitrary orientation. Optimization techniques which consider the hood geometry were investigated. The identified technique can be used to select hood orifice shape and dimensions not only to achieve proper control but also improve the mechanical efficiency of the process.

17. Document Analysis a. Descriptors

b. Identifiers/Open-Ended Terms NIOSH-Publication, NIOSH-Grant, Grant-Number-R01-OH-02132, End-Date-12-31-1989, Control-technology, Exhaust-hoods, Air-flow, Ventilation-equipment, Ventilation-systems

c. COSATI Field/Group

18. Availability Statement	19. Security Class (This Report)	21. No. of Pages 114
	22. Security Class (This Page)	22. Price

(See ANSI-Z39.18) *See Instructions on Reverse* **OPTIONAL FORM 272(4-77)** (Formerly NTIS-35) Department of Commerce